

Fast and Flexible Neutrino Decoupling Part I: The Standard Model

M. Escudero ^{1,*} G. Jackson ^{2,†} M. Laine ^{3,‡} and S. Sandner ^{4,§}

¹*Theoretical Physics Department, CERN, 1 Esplanade des Particules, CH-1211 Geneva 23, Switzerland*

²*SUBATECH UMR 6457 (IMT Atlantique, Nantes Université, IN2P3/CNRS),
4 rue Alfred Kastler, 44307 Nantes, France*

³*AEC, Institute for Theoretical Physics, University of Bern, Sidlerstrasse 5, CH-3012 Bern, Switzerland*

⁴*Theoretical Division, Los Alamos National Laboratory, Los Alamos, NM 87545, USA*

Cosmological determinations of the number of relativistic neutrino species, N_{eff} , are becoming increasingly accurate, and further improvements are expected both from CMB and BBN data. Given this context, we update the evaluation of N_{eff} and the current entropy density via the momentum-averaged approach. This allows for a numerically fast description of neutrino decoupling, easily portable to an array of new physics scenarios. We revisit all aspects of this approach, including collision terms with full electron mass dependence, finite temperature QED corrections to the equation of state, neutrino oscillations, and the modelling of neutrino ensembles with effective chemical potentials. For integrated observables, our results differ by less than 0.04% from the solution of the momentum-dependent evolution equation. We outline how to extend the approach to BSM settings, and will highlight its power in Part II. To facilitate the practical implementation, we release a **Mathematica** and **python** code within `nudec_BSM_v2` [Github](#) , easily linkable to BBN codes.

CONTENTS

1. Introduction	2
2. Basic variables, rate equations and rate coefficients	3
A. Outline of the momentum-averaged approach	3
B. Determination of rate coefficients via matching to linear-response regime	5
3. Inclusion of dynamical oscillations in the momentum-averaged approach	8
4. QED corrections to energy density and pressure	9
5. Parametrization of the universe expansion in terms of N_{eff} and h_{eff}	10
6. Main results and their comparison with the Liouville equation	11
7. Outline of BSM extensions	14
8. Notes on numerical codes and data tables	14
9. Conclusions	15
A. Couplings and matrix elements squared	17
B. Parametrization of the rate coefficients	18
C. Comparison in the Standard Model: momentum-averaged vs. Liouville solution	18
D. QED equation of state	21
E. Bessel and polylogarithmic representations of thermodynamic quantities	27
References	31

* miguel.escudero@cern.ch

† jackson@subatech.in2p3.fr

‡ laine@itp.unibe.ch

§ stefan.sandner@lanl.gov

1. INTRODUCTION

The measurement of the effective number of relativistic neutrino species, N_{eff} , from Cosmic Microwave Background (CMB) observations has improved at an impressive pace over the last 15 years:

$$\begin{aligned} N_{\text{eff}} &> 2.3 \text{ at 95% CL} & (2008) \text{ WMAP-5 [1]}, \\ N_{\text{eff}} &= 3.66 \pm 0.34 & (2013) \text{ Planck + WMAP [2]}, \\ N_{\text{eff}} &= 2.92 \pm 0.19 & (2018) \text{ Planck [3]}, \\ N_{\text{eff}} &= 2.81 \pm 0.12 & (2025) \text{ Planck + ACT + SPT-3G [4–6]}. \end{aligned}$$

Further improvements are expected from SPT-3G+ [7] (± 0.07) and the Simons Observatory [8] (± 0.05). In parallel, inferences of the expansion rate from Big Bang Nucleosynthesis (BBN) have improved in the past ~ 20 years due to a more robust measurement of the primordial helium abundance [9, 10], a 1% determination of the primordial deuterium abundance [11], and better knowledge about nuclear reaction rates that control the deuterium abundance [12–15].

Independently, there has been increased interest in particles beyond the Standard Model (SM) which are lighter than the weak scale and which can affect N_{eff} and BBN. Well-motivated scenarios include MeV-scale thermal dark matter particles [16–20], hidden photons [21–25], dark scalars [26–29], axions [30–34], sterile neutrinos [35–37], and many others, see e.g. refs. [38–40] for extensive discussions.

In this context, it is important to have flexible tools to explore the phenomenology of extensions of the Standard Model that can modify N_{eff} and BBN. This entails solving for the process of neutrino decoupling, which occurred when the universe was $t \sim 1$ s old and had a temperature of about $T_\gamma \sim 1$ MeV. At this point the electroweak interactions that kept neutrinos in thermal equilibrium stopped being efficient. Soon afterwards, at $T_\gamma \sim m_e$, electrons and positrons became non-relativistic and their decays released more energy to photons than to neutrinos, leading to the famous $T_\gamma/T_\nu \simeq 1.4$ ratio. Solving for this process requires tracking the evolution of neutrinos, of the electromagnetic plasma, and of the exchanges of energy, momentum, and particle number between them.

The most precise approach to calculate the process of neutrino decoupling is to solve for the neutrino density matrix using the momentum-dependent Liouville equation that takes into account the neutrino-neutrino and neutrino-electron interactions [41–45]. With a comoving momentum grid, this leads to $\mathcal{O}(100)$ coupled non-linear integro-differential equations which are stiff and thus challenging to track numerically, see e.g. refs. [42, 45]. The issue becomes worse in many extensions of the Standard Model, because new physics states can interact with neutrinos at rates much larger than the Hubble rate. This implies a scale hierarchy, making solving the Liouville equation even harder. On the other hand, a large interaction rate leads to rapid equilibration, and then we already know the shape of the corresponding distribution function, suggesting that there is no need to track it dynamically.¹

The idea to insert a thermal shape for a distribution function, parametrized by a temperature and a chemical potential, has a long history. It was already used for pioneering recombination calculations [51, 52], and is commonly employed in WIMP literature to calculate the evolution of thermal relics [53, 54], because their kinetic equilibration rate is much faster than the chemical one. However, it was also used to provide early estimates of N_{eff} in the Standard Model [55–58], and was more recently exploited for BSM scenarios in the context of neutrino decoupling [59, 60]. The approach is fast, flexible, and sufficiently accurate for many practical purposes, which has motivated new BBN codes to adopt it [61, 62].

While refs. [59, 60] introduced the essential elements to solve for neutrino decoupling in the presence of new thermal relics, several approximations and simplifications were adopted. The main goal of the present paper and its companion [63] is to scrutinize and significantly improve upon these works. The improvements are:

1. *Updated neutrino-electron interaction rates in the Standard Model.* The interaction rates used in refs. [59, 60] employed the massless electron limit and assumed Maxwell-Boltzmann statistics for neutrinos and electrons. In this study we calculate the rates exactly at leading order (LO) in α_{em} , and provide an accurate linear response representation of the full mass dependence and also featuring non-zero chemical potentials. The new rates are more flexible and accurate than the previous ones, but remain simple and compact.

¹ We note that the Liouville equation also becomes hard to solve if high-energy neutrinos are injected, as happens for instance in the case of GeV-scale sterile neutrinos [37]. For these types of scenarios, a recently developed method using direct Monte Carlo sampling of the collisions [46, 47] has been shown to give very good results, both in the Standard Model [48] and beyond [49, 50].

2. *Increased computational speed.* The thermodynamic formulae for the number and energy densities used in refs. [59, 60] were integrated over momentum explicitly, which led to a significant computational cost. Here, inspired by the implementation of some BBN codes [62, 64–66], we make use of accurate low-temperature expansions in terms of Bessel functions. This yields a speed-up of about a factor of 10, without any loss of precision (provided that effective chemical potentials are small or negative, which is the typical case).
3. *Exploration of neutrino oscillations.* Given the observed mass differences and mixing angles, neutrinos start to oscillate at $T \sim 10$ MeV in the early universe. While physically important, this effect is numerically small in the Standard Model calculation for N_{eff} , and for simplicity refs. [59, 60] did not account for it. It was rather argued that given the rapid neutrino oscillations, the ν_e , ν_μ and ν_τ neutrinos effectively share a common temperature. Here we do include oscillations, and demonstrate that they only have a small effect in the Standard Model, while improving on the match to the full Liouville solution. In our companion paper [63], we study the issue in BSM settings, with particles interacting at different rates with different neutrino species.
4. *Accuracy of the approach and spectral distortions.* At the time of refs. [59, 60] there were only a handful of high-accuracy solutions to the Liouville equation, but a resurgence of interest in N_{eff} led to a consensus N_{eff} calculation by several groups [67–69]. In this work, by comparing against the public code `FortEPiaNO` [70], we provide a comparison between the full Liouville solution and that assuming thermally shaped distribution functions. This enables us to understand what are the spectral distortions of the Cosmic Neutrino Background as well as the accuracy of the momentum-averaged approach to solve for neutrino decoupling.
5. *Higher-order QED corrections to the energy density and pressure of the plasma.* State-of-the-art calculations of N_{eff} implement the $\mathcal{O}(e^2)$ [71, 72] and $\mathcal{O}(e^3)$ [73] QED thermal corrections (cf. ref. [74] and references therein) to the electromagnetic energy density of the universe, as this leads to a change $\Delta N_{\text{eff}} \sim 0.01$. Here we recalculate and re-implement these corrections, and estimate the $\mathcal{O}(e^4)$ and $\mathcal{O}(e^5)$ ones. We show that though the last ones introduce qualitatively new structures, they are numerically small and can be safely neglected.

Our study is structured as follows. First, in sec. 2, we review the basic ingredients for the solution of neutrino decoupling using a momentum-averaged approach. We introduce our newly developed collision terms, and write simple versions thereof using a linear response approach. In sec. 3, we show how neutrino oscillations can be incorporated in the momentum-averaged approach. In sec. 4, we present a new calculation of the QED equation of state featuring corrections up to $\mathcal{O}(e^5)$. In sec. 5, we define the physical observables extracted from the solution. In sec. 6, we compare our results against the solution of the momentum-dependent Liouville equation. In sec. 7, we anticipate how the framework can be extended to include BSM particles. In sec. 8, we briefly summarize the codes and data tables that accompany this work, before concluding in sec. 9. Several details are relegated to a number of appendices, including a quantification of spectral distortions of the Cosmic Neutrino Background.

2. BASIC VARIABLES, RATE EQUATIONS AND RATE COEFFICIENTS

Neutrinos interact with electrons, positrons and themselves in the early universe, via the processes $\nu\bar{\nu} \leftrightarrow e^+e^-$, $\nu e^\pm \rightarrow \nu e^\pm$, $\nu\bar{\nu} \rightarrow \nu\bar{\nu}$, and $\nu\nu \rightarrow \nu\nu$. The rates of these interactions drop below the Hubble rate at $T_\gamma < 2$ MeV. Soon afterwards, at around $T_\gamma \sim m_e$, electrons and positrons become non-relativistic, and the energy released in their decays is mostly taken up by photons. In this section, we describe how to track this system in the momentum-averaged approach, which assumes that all particles follow thermally shaped distribution functions.

A. Outline of the momentum-averaged approach

In the momentum-averaged approach, we think of the system as consisting of a number of separate subsystems. These include a QED plasma and the neutrino and antineutrino ensembles, but generically also other sectors depending on the new physics scenario considered (see sec. 7 and ref. [63]). Focusing on the Standard Model for the moment,

energy-momentum conservation equations for the subsystems can be written as

$$\frac{d\rho_i}{dt} + 3H(\rho_i + p_i) = Q_i, \quad \sum_i Q_i = 0, \quad i \in \{\text{em}, \nu_e, \nu_\mu, \nu_\tau\}, \quad (2.1)$$

where H is the Hubble rate, ρ_i denote energy densities, p_i pressures, Q_i energy transfer rates, and “em” refers to the entire QED ensemble formed of electrons, positrons and photons (we disregard baryons as their density is negligible at $T_\gamma \sim \text{MeV}$). We assume that there are no substantial lepton asymmetries, so that the neutrino and antineutrino ensembles can be treated as equivalent; and that neutrino oscillations are either very slow or very fast compared to the interaction rate (we return to dynamical neutrino oscillations in sec. 3). Given that neutrino number densities, n_i , are slowly evolving, we can also write down the corresponding evolution equations,

$$\frac{dn_i}{dt} + 3Hn_i = J_i, \quad i \in \{\nu_e, \nu_\mu, \nu_\tau\}, \quad (2.2)$$

where the source terms, J_i , originate from the same Fermi vertices (cf. appendix A) as the energy transfer rates, Q_i .

As the universe cools down, neutrinos eventually fall out of equilibrium with the QED plasma. The essence of the momentum-averaged approach is to parametrize their distribution functions by two quantities, an effective temperature (T_i) and an effective chemical potential (μ_i).² We can then write $\dot{\rho}_i = (\partial\rho_i/\partial T_i)\dot{T}_i + (\partial\rho_i/\partial\mu_i)\dot{\mu}_i$, and correspondingly for \dot{n}_i . Inserting these in eqs. (2.1) and (2.2), we can solve for the time dependence of the effective temperatures and chemical potentials,

$$\frac{dT_i}{dt} = \frac{-3H\left((\rho_i + p_i)\frac{\partial n_i}{\partial\mu_i} - n_i\frac{\partial\rho_i}{\partial\mu_i}\right) + Q_i\frac{\partial n_i}{\partial\mu_i} - J_i\frac{\partial\rho_i}{\partial\mu_i}}{\frac{\partial n_i}{\partial\mu_i}\frac{\partial\rho_i}{\partial T_i} - \frac{\partial n_i}{\partial T_i}\frac{\partial\rho_i}{\partial\mu_i}}, \quad (2.3a)$$

$$\frac{d\mu_i}{dt} = \frac{3H\left((\rho_i + p_i)\frac{\partial n_i}{\partial T_i} - n_i\frac{\partial\rho_i}{\partial T_i}\right) - Q_i\frac{\partial n_i}{\partial T_i} + J_i\frac{\partial\rho_i}{\partial T_i}}{\frac{\partial n_i}{\partial\mu_i}\frac{\partial\rho_i}{\partial T_i} - \frac{\partial n_i}{\partial T_i}\frac{\partial\rho_i}{\partial\mu_i}}. \quad (2.3b)$$

For the QED plasma, which has a negligible chemical potential, the evolution equation from eq. (2.1) reads³

$$\frac{dT_\gamma}{dt} = \frac{-3H(\rho_{\text{em}} + p_{\text{em}}) + Q_{\text{em}}}{\frac{d\rho_{\text{em}}}{dT_\gamma}}. \quad (2.6)$$

The system of equations is completed by an equation for the Hubble rate,

$$H^2 \equiv \frac{\dot{a}^2}{a^2} = \frac{8\pi}{3}\frac{\rho_t}{m_{\text{pl}}^2}, \quad \rho_t \equiv \sum_i \rho_i, \quad (2.7)$$

where a is the scale factor, ρ_t the overall energy density, and $m_{\text{pl}} = 1.2209 \times 10^{19} \text{ GeV}$ the Planck mass.

² This μ_i should not be confused with a chemical potential parametrizing particle-antiparticle asymmetries, but rather refers to a distortion of the equilibrium Fermi-Dirac distribution, as defined in eq. (2.10).

³ To connect with the notation in refs. [59, 60], we recall that it is common to separate the Stefan-Boltzmann contributions from photons (γ) and electrons and positrons (e) from the interaction part (int). In the last we can employ the thermodynamic identities $\rho_{\text{int}} + p_{\text{int}} = T_\gamma dp_{\text{int}}/dT_\gamma$ and $dp_{\text{int}}/dT_\gamma = T_\gamma d^2p_{\text{int}}/dT_\gamma^2$, valid because the baryon chemical potential is negligible. Then

$$\frac{dT_\gamma}{dt} \stackrel{(2.6)}{=} -\frac{4H\rho_\gamma + 3H(\rho_e + p_e) + 3H T_\gamma \frac{dp_{\text{int}}}{dT_\gamma} - Q_{\text{em}}}{\frac{d\rho_\gamma}{dT_\gamma} + \frac{dp_e}{dT_\gamma} + T_\gamma \frac{d^2p_{\text{int}}}{dT_\gamma^2}}. \quad (2.4)$$

For neutrinos with $\mu_i \ll T_i$, eqs. (E.9a) and (E.9b) imply $n_i \approx bT_i^3 + c\mu_i T_i^2$ and $3p_i = \rho_i \approx dT_i^4 + 3b\mu_i T_i^3$, where b, c and d are constants. Then $\Delta_i \equiv \frac{\partial n_i}{\partial\mu_i}\frac{\partial\rho_i}{\partial T_i} - \frac{\partial n_i}{\partial T_i}\frac{\partial\rho_i}{\partial\mu_i} \approx (4cd - 9b^2)T_i^5$, $(\rho_i + p_i)\frac{\partial n_i}{\partial\mu_i} - n_i\frac{\partial\rho_i}{\partial\mu_i} \approx T_i\Delta_i/3$ and $(\rho_i + p_i)\frac{\partial n_i}{\partial T_i} - n_i\frac{\partial\rho_i}{\partial T_i} \approx -\mu_i\Delta_i/3$, whereby

$$\frac{dT_i}{dt} \stackrel{(2.3a)}{\approx} -HT_i + \frac{Q_i\frac{\partial n_i}{\partial\mu_i} - J_i\frac{\partial\rho_i}{\partial\mu_i}}{\Delta_i} \stackrel{\text{no } n_i, \mu_i}{\approx}_{(2.1)} -HT_i + \frac{Q_i}{d\rho_i/dT_i}, \quad \frac{d\mu_i}{dt} \stackrel{(2.3b)}{\approx} -H\mu_i - \frac{Q_i\frac{\partial n_i}{\partial T_i} - J_i\frac{\partial\rho_i}{\partial T_i}}{\Delta_i}. \quad (2.5)$$

Apart from the temperatures and chemical potentials, it is also interesting to determine how many *e-folds*, $\mathcal{N} \equiv \ln a$, take place during the decoupling period (cf. sec. 5). For this we need to integrate $\dot{\mathcal{N}} = H$. However, the evolution of a correlates strongly with the redshift of the temperatures, so it is simpler to consider

$$z \equiv \frac{aT_\gamma}{(aT_\gamma)_{\text{ini}}} , \quad \dot{z} = z \left(H + \frac{\dot{T}_\gamma}{T_\gamma} \right) , \quad (2.8)$$

where $(\dots)_{\text{ini}}$ denotes some initial value well before the decoupling process starts (cf. eq. (8.1)). We remark that z does not influence the solution of eqs. (2.3)–(2.6), but it can be obtained as their by-product.

In order to compute the coefficients Q_i and J_i that appear in eqs. (2.3)–(2.6), we need to parametrize the underlying neutrino and antineutrino density matrices, ϱ_ν , in terms of T_i and μ_i . Assuming the system to be homogeneous, and denoting by \mathbf{q} a physical momentum, with $q \equiv |\mathbf{q}|$, the density matrix (in the flavour basis) is assumed to take the form

$$\varrho_\nu(t, \mathbf{q}) = \begin{cases} \begin{pmatrix} f_{\nu_e}(t, q) & & \\ & f_{\nu_\mu}(t, q) & \\ & & f_{\nu_\tau}(t, q) \end{pmatrix} & [\text{"no oscillations"}] , \\ f_\nu(t, q) \begin{pmatrix} 1 & & \\ & 1 & \\ & & 1 \end{pmatrix} & [\text{"fast oscillations"}] . \end{cases} \quad (2.9)$$

Here the diagonal entries are assumed to take the *equilibrium* Fermi-Dirac shape for *massless* neutrinos,

$$f_{\nu_\alpha} \equiv f_{\bar{\nu}_\alpha} \equiv [e^{(q-\mu_{\nu_\alpha})/T_{\nu_\alpha}} + 1]^{-1} . \quad (2.10)$$

In practice, the ν_μ and ν_τ flavours are treated as degenerate, and they are denoted by ν_μ . The generalization of eq. (2.9) to include neutrino oscillations is given in eq. (3.5).

Given the form in eq. (2.9), the neutrino energy densities, pressures, and number densities that appear in eqs. (2.3a) and (2.3b) read

$$\rho_{\nu_\alpha} = 2 \int_{\mathbf{q}} q f_{\nu_\alpha} , \quad p_{\nu_\alpha} = 2 \int_{\mathbf{q}} \frac{q f_{\nu_\alpha}}{3} = -2T_{\nu_\alpha} \int_{\mathbf{q}} \ln(1 - f_{\nu_\alpha}) , \quad n_{\nu_\alpha} = 2 \int_{\mathbf{q}} f_{\nu_\alpha} , \quad (2.11)$$

where the factor 2 counts the left-handed neutrinos and right-handed antineutrinos; $\int_{\mathbf{q}} = (2\pi^2)^{-1} \int_0^\infty dq q^2$; and for p_{ν_a} we have shown two versions related by partial integration. The integrals in eq. (2.11) can be carried out in terms of polylogarithms, as summarized in appendix E. We remark that neutrinos have a vanishing trace anomaly in this massless and non-interacting limit, $\rho_{\nu_a} - 3p_{\nu_a} = 0$. The QED energy density and pressure, ρ_{em} and p_{em} , have more structure, and we return to them in sec. 4 and in appendix D.

B. Determination of rate coefficients via matching to linear-response regime

In the momentum-averaged approach of sec. 2A, the interactions of the neutrino and QED ensembles are modelled by energy density transfer rates (Q_i) and number density transfer rates (J_i). These rates refer to the given density going to the destination ensemble, but they are a sum over all sources. In the following, in order to streamline the notation, we first consider the partial contributions $Q \equiv Q_{\nu_\alpha \leftarrow \text{em}}$ and $J \equiv J_{\nu_\alpha \leftarrow \text{em}}$. We return to the neutrino-neutrino rates at the end of this section (cf. eqs. (2.27)–(2.30)).

If two ensembles are in thermal equilibrium with each other, the rate coefficients vanish, as required by detailed balance. Therefore, quite generally, the values of the coefficients are of *first order* in the differences of the characteristics of the neutrino and QED ensembles. However, as the universe cools down, in the end the two ensembles differ from each other by effects of $\mathcal{O}(1)$. To describe the whole decoupling process, we need approximate expressions for Q and J also *beyond the linear order*. In the following, we describe how such expressions can be obtained, by combining a

strict linear response philosophy with a phenomenological Maxwell-Boltzmann (MB) approximation.

If we introduce the kinematic Maxwell-Boltzmann approximation for describing the phase-space distributions of electrons, and furthermore treat the electrons as massless ($m_e = 0$) for a moment, then Q and J can be computed exactly at LO in α_{em} . The expressions read [60]

$$Q^{\text{MB}} \equiv \frac{32G_F^2}{\pi^5} (g_{\alpha L}^2 + g_{\alpha R}^2) \left[4 \underbrace{(T_\gamma^9 - T_\nu^9 e^{\frac{2\mu_\nu}{T_\nu}})}_{\text{gain-loss}} + 7 \underbrace{T_\gamma^4 T_\nu^4 (T_\gamma - T_\nu) e^{\frac{\mu_\nu}{T_\nu}}}_{\text{scattering}} \right], \quad (2.12a)$$

$$J^{\text{MB}} \equiv \frac{32G_F^2}{\pi^5} (g_{\alpha L}^2 + g_{\alpha R}^2) \underbrace{(T_\gamma^8 - T_\nu^8 e^{\frac{2\mu_\nu}{T_\nu}})}_{\text{gain-loss}}, \quad (2.12b)$$

where the physical origin of each term has been indicated. Scatterings do not transfer particle number while pair creations and annihilations (“gain–loss”) do. The values of the couplings used are collected in appendix A.

Now, if we go beyond the Maxwell-Boltzmann approximation, and include $m_e \neq 0$ in the computation, the functional forms of Q and J become more complicated, and cannot be written analytically. However, the result of any computation can still be expanded to first order around equilibrium. So, let us define

$$\frac{T_\nu}{T_\gamma} \equiv 1 + \epsilon_T + \mathcal{O}(\epsilon^2), \quad \frac{\mu_\nu}{T_\nu} \equiv \epsilon_\mu + \mathcal{O}(\epsilon^2). \quad (2.13)$$

Then, to facilitate the linearisation, we can express the full leading-order (LO) transfer rates as

$$\frac{Q^{\text{LO}}}{T_\gamma^9 G_F^2} = \frac{1}{\pi^5} \left\{ (g_{\alpha L}^2 + g_{\alpha R}^2) \widehat{Q}_1 \left(\frac{T_\nu}{T_\gamma}, \frac{\mu_\nu}{T_\nu}; \frac{m_e}{T_\gamma} \right) + g_{\alpha L} g_{\alpha R} \widehat{Q}_2 \left(\frac{T_\nu}{T_\gamma}, \frac{\mu_\nu}{T_\nu}; \frac{m_e}{T_\gamma} \right) \right\}, \quad (2.14)$$

$$\frac{J^{\text{LO}}}{T_\gamma^8 G_F^2} = \frac{1}{\pi^5} \left\{ (g_{\alpha L}^2 + g_{\alpha R}^2) \widehat{J}_1 \left(\frac{T_\nu}{T_\gamma}, \frac{\mu_\nu}{T_\nu}; \frac{m_e}{T_\gamma} \right) + g_{\alpha L} g_{\alpha R} \widehat{J}_2 \left(\frac{T_\nu}{T_\gamma}, \frac{\mu_\nu}{T_\nu}; \frac{m_e}{T_\gamma} \right) \right\}, \quad (2.15)$$

where \widehat{Q} and \widehat{J} are dimensionless functions of dimensionless variables. The terms proportional to $g_{\alpha L} g_{\alpha R}$ arise when $m_e \neq 0$ (cf. eq. (A.6)). The LO functions can be decomposed into “gain–loss” and “scattering” parts, as done in eqs. (2.12a) and (2.12b). After inserting eq. (2.13) into Q^{LO} and expanding, the leading terms in the expansion vanish due to the equilibrium condition. Thus we obtain, e.g.,

$$\frac{Q^{\text{LO}}}{T_\gamma^9 G_F^2} = \frac{1}{\pi^5} \left\{ (g_{\alpha L}^2 + g_{\alpha R}^2) \left[\epsilon_T \widehat{Q}_1^{(1,0)} + \epsilon_\mu \widehat{Q}_1^{(0,1)} \right] + g_{\alpha L} g_{\alpha R} \left[\epsilon_T \widehat{Q}_2^{(1,0)} + \epsilon_\mu \widehat{Q}_2^{(0,1)} \right] \right\} + \mathcal{O}(\epsilon_T^2, \epsilon_T \epsilon_\mu, \epsilon_\mu^2), \quad (2.16)$$

where we introduced the following coefficients for $i = \{1, 2\}$, which are functions of m_e/T_γ alone,

$$\widehat{Q}_i^{(1,0)} \equiv \partial_{T_\nu} \widehat{Q}_i \left(\frac{T_\nu}{T_\gamma}, \frac{\mu_\nu}{T_\nu}; \frac{m_e}{T_\gamma} \right) \Big|_{T_\nu=T_\gamma, \mu_\nu=0}, \quad (2.17)$$

$$\widehat{Q}_i^{(0,1)} \equiv \partial_{\mu_\nu} \widehat{Q}_i \left(\frac{T_\nu}{T_\gamma}, \frac{\mu_\nu}{T_\nu}; \frac{m_e}{T_\gamma} \right) \Big|_{T_\nu=T_\gamma, \mu_\nu=0}. \quad (2.18)$$

A similar expression can be obtained for J^{LO} in eq. (2.15), which then involves the coefficients $\widehat{J}_i^{(1,0)}$ and $\widehat{J}_i^{(0,1)}$. The same strategy can also be employed at higher orders in α_{em} , though for the moment complete results are only available in the $m_e = 0$ limit [75, 76].

In order to extend eqs. (2.12a) and (2.12b) in the most general way, as allowed by the linearisation provided by eq. (2.16), we introduce m_e -dependent correction factors as

$$(g_{\alpha L}^2 + g_{\alpha R}^2) (T_\gamma^9 - T_\nu^9 e^{2\frac{\mu_\nu}{T_\nu}}) \rightarrow \left[(g_{\alpha L}^2 + g_{\alpha R}^2) f_{a1} \left(\frac{m_e}{T_\gamma} \right) + g_{\alpha L} g_{\alpha R} f_{a2} \left(\frac{m_e}{T_\gamma} \right) \right] (T_\gamma^9 - T_\nu^9 e^{2\frac{\mu_\nu}{T_\nu}})$$

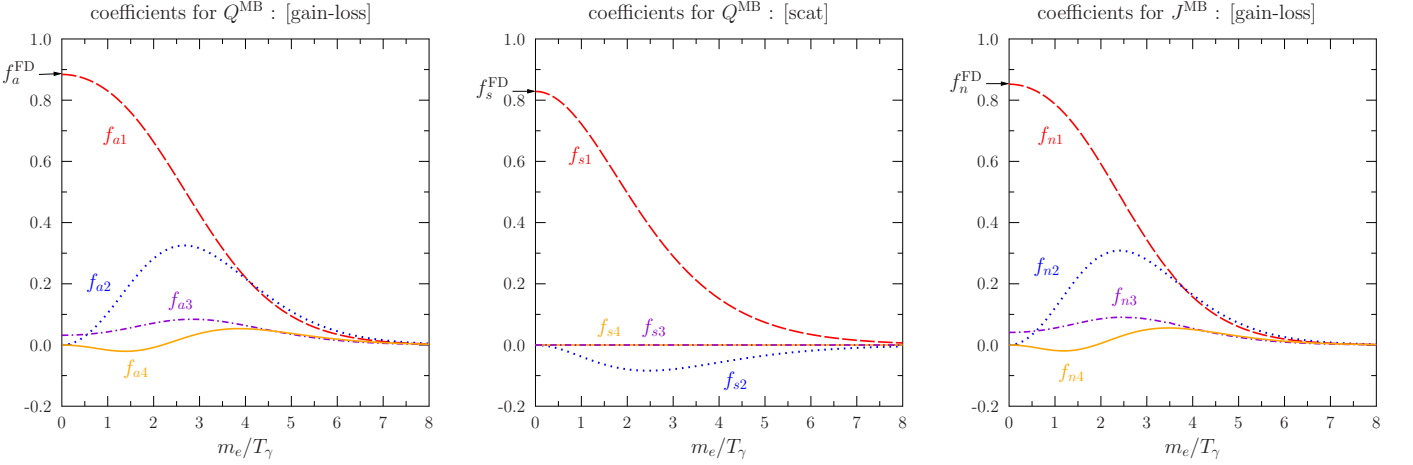


FIG. 1. The MB correction factors for the energy density and number density transfer rates, determined by matching to the linear response regime. These correct eqs. (2.12a) and (2.12b) as laid out by the replacements in eqs. (2.19)–(2.21).

$$+ \left[(g_{\alpha L}^2 + g_{\alpha R}^2) f_{a3}\left(\frac{m_e}{T_\gamma}\right) + g_{\alpha L} g_{\alpha R} f_{a4}\left(\frac{m_e}{T_\gamma}\right) \right] \sqrt{T_\gamma^9 T_\nu^9} (e^{2\frac{\mu_\nu}{T_\nu}} - 1) , \quad (2.19)$$

$$(g_{\alpha L}^2 + g_{\alpha R}^2) T_\gamma^4 T_\nu^4 (T_\gamma - T_\nu) e^{\frac{\mu_\nu}{T_\nu}} \rightarrow \left[(g_{\alpha L}^2 + g_{\alpha R}^2) f_{s1}\left(\frac{m_e}{T_\gamma}\right) + g_{\alpha L} g_{\alpha R} f_{s2}\left(\frac{m_e}{T_\gamma}\right) \right] T_\gamma^4 T_\nu^4 (T_\gamma - T_\nu) e^{\frac{\mu_\nu}{T_\nu}} \\ + \left[(g_{\alpha L}^2 + g_{\alpha R}^2) f_{s3}\left(\frac{m_e}{T_\gamma}\right) + g_{\alpha L} g_{\alpha R} f_{s4}\left(\frac{m_e}{T_\gamma}\right) \right] \sqrt{T_\gamma^9 T_\nu^9} (e^{\frac{\mu_\nu}{T_\nu}} - 1) , \quad (2.20)$$

$$(g_{\alpha L}^2 + g_{\alpha R}^2) (T_\gamma^8 - T_\nu^8 e^{2\frac{\mu_\nu}{T_\nu}}) \rightarrow \left[(g_{\alpha L}^2 + g_{\alpha R}^2) f_{n1}\left(\frac{m_e}{T_\gamma}\right) + g_{\alpha L} g_{\alpha R} f_{n2}\left(\frac{m_e}{T_\gamma}\right) \right] (T_\gamma^8 - T_\nu^8 e^{2\frac{\mu_\nu}{T_\nu}}) \\ + \left[(g_{\alpha L}^2 + g_{\alpha R}^2) f_{n3}\left(\frac{m_e}{T_\gamma}\right) + g_{\alpha L} g_{\alpha R} f_{n4}\left(\frac{m_e}{T_\gamma}\right) \right] T_\gamma^4 T_\nu^4 (e^{2\frac{\mu_\nu}{T_\nu}} - 1) . \quad (2.21)$$

In the second lines of these equations, we chose to employ a temperature dependence symmetric in T_γ and T_ν (this will be convenient shortly, when we consider also the transfers between the neutrino ensembles).

We can then match linear-response versions of eqs. (2.19)–(2.21) to eq. (2.16), thereby determining the unknown functions. The results are given in appendix B, and illustrated numerically in fig. 1. The non-zero values for $m_e/T_\gamma = 0$ are $f_{a1}(0) = 0.884$, $f_{s1}(0) = 0.829$, $f_{n1}(0) = 0.829$, $f_{a3}(0) = 0.032$, and $f_{n3}(0) = 0.041$. Furthermore, f_{s3} and f_{s4} are identically zero for any m_e , indicating that there is no order ϵ_ν term in the expansion of $Q_{\text{scattering}}^{\text{LO}}$. This fact can be shown quite generally⁴ by observing that \hat{Q}_i vanishes when $T_\nu = T_\gamma$, for any value of μ_ν and m_e .

We now return to the general matrix structure of the rate coefficients. Supplementing eqs. (2.19)–(2.21) by the contributions of the other neutrino ensembles, we can write down full rates for a neutrino of a given flavour α . In order to do so, we introduce the functions

$$F_a^{12}(T_A, T_B, \mu_A, \mu_B) \equiv T_A^9 e^{2\frac{\mu_A}{T_B}} - T_B^9 e^{2\frac{\mu_B}{T_A}} , \quad (2.22)$$

$$F_a^{34}(T_A, T_B, \mu_A, \mu_B) \equiv (T_A^9 T_B^9)^{\frac{1}{2}} (e^{2\frac{\mu_B}{T_B}} - e^{2\frac{\mu_A}{T_A}}) , \quad (2.23)$$

$$F_s^{12}(T_A, T_B, \mu_A, \mu_B) \equiv T_A^4 T_B^4 (T_A - T_B) e^{\frac{\mu_A}{T_A}} e^{\frac{\mu_B}{T_B}} , \quad (2.24)$$

⁴ The proof relies on detailed balance, as well as exchanging integration variables, and it should be true even if $\mu_{\bar{\nu}} \neq \mu_\nu$.

$$F_n^{12}(T_A, T_B, \mu_A, \mu_B) \equiv T_A^8 e^{2\frac{\mu_A}{T_A}} - T_B^8 e^{2\frac{\mu_B}{T_B}}, \quad (2.25)$$

$$F_n^{34}(T_A, T_B, \mu_A, \mu_B) \equiv T_A^4 T_B^4 (e^{2\frac{\mu_B}{T_B}} - e^{2\frac{\mu_A}{T_A}}). \quad (2.26)$$

The subscript and superscript in F refer to which mass-dependent correction the structure concerns (cf. eqs. (2.19)–(2.21)). By construction, these functions are odd under the simultaneous exchange $T_A \leftrightarrow T_B$ and $\mu_A \leftrightarrow \mu_B$, ensuring that the partial rates satisfy $Q_{i \leftarrow j} = -Q_{j \leftarrow i}$ and vanish in equilibrium. The mutual exchanges among the QED and neutrino systems can then be written as

$$\begin{aligned} Q_{\nu_\alpha \leftarrow \text{em}} &= \frac{32G_F^2}{\pi^5} \left\{ 4 \times \left[\left((g_{\alpha L}^2 + g_{\alpha R}^2) f_{a1}\left(\frac{m_e}{T_\gamma}\right) + g_{\alpha L} g_{\alpha R} f_{a2}\left(\frac{m_e}{T_\gamma}\right) \right) F_a^{12}(T_\gamma, T_{\nu_\alpha}, 0, \mu_{\nu_\alpha}) \right. \right. \\ &\quad \left. \left. + \left((g_{\alpha L}^2 + g_{\alpha R}^2) f_{a3}\left(\frac{m_e}{T_\gamma}\right) + g_{\alpha L} g_{\alpha R} f_{a4}\left(\frac{m_e}{T_\gamma}\right) \right) F_a^{34}(T_\gamma, T_{\nu_\alpha}, 0, \mu_{\nu_\alpha}) \right] \right. \\ &\quad \left. + 7 \times \left[(g_{\alpha L}^2 + g_{\alpha R}^2) f_{s1}\left(\frac{m_e}{T_\gamma}\right) + g_{\alpha L} g_{\alpha R} f_{s2}\left(\frac{m_e}{T_\gamma}\right) \right] F_s^{12}(T_\gamma, T_{\nu_\alpha}, 0, \mu_{\nu_\alpha}) \right\}, \end{aligned} \quad (2.27)$$

$$\begin{aligned} Q_{\nu_\alpha \leftarrow \nu_\beta} &= \frac{8G_F^2}{\pi^5} \left\{ 4 \times \left[f_{a1}(0) F_a^{12}(T_{\nu_\beta}, T_{\nu_\alpha}, \mu_{\nu_\beta}, \mu_{\nu_\alpha}) + f_{a3}(0) F_a^{34}(T_{\nu_\beta}, T_{\nu_\alpha}, \mu_{\nu_\beta}, \mu_{\nu_\alpha}) \right] \right. \\ &\quad \left. + 7 f_{s1}(0) F_s^{12}(T_{\nu_\beta}, T_{\nu_\alpha}, \mu_{\nu_\beta}, \mu_{\nu_\alpha}) \right\}, \end{aligned} \quad (2.28)$$

$$\begin{aligned} J_{\nu_\alpha \leftarrow \text{em}} &= \frac{32G_F^2}{\pi^5} \left[\left((g_{\alpha L}^2 + g_{\alpha R}^2) f_{n1}\left(\frac{m_e}{T_\gamma}\right) + g_{\alpha L} g_{\alpha R} f_{n2}\left(\frac{m_e}{T_\gamma}\right) \right) F_n^{12}(T_\gamma, T_{\nu_\alpha}, 0, \mu_{\nu_\alpha}) \right. \\ &\quad \left. + \left((g_{\alpha L}^2 + g_{\alpha R}^2) f_{n3}\left(\frac{m_e}{T_\gamma}\right) + g_{\alpha L} g_{\alpha R} f_{n4}\left(\frac{m_e}{T_\gamma}\right) \right) F_n^{34}(T_\gamma, T_{\nu_\alpha}, 0, \mu_{\nu_\alpha}) \right], \end{aligned} \quad (2.29)$$

$$J_{\nu_\alpha \leftarrow \nu_\beta} = \frac{8G_F^2}{\pi^5} \left[f_{n1}(0) F_n^{12}(T_{\nu_\beta}, T_{\nu_\alpha}, \mu_{\nu_\beta}, \mu_{\nu_\alpha}) + f_{n3}(0) F_n^{34}(T_{\nu_\beta}, T_{\nu_\alpha}, \mu_{\nu_\beta}, \mu_{\nu_\alpha}) \right]. \quad (2.30)$$

The specific transfer rates introduced in eqs. (2.1) and (2.2) are given in terms of these partial rates as

$$Q_{\nu_\alpha} = Q_{\nu_\alpha \leftarrow \text{em}} + \sum_{\beta \neq \alpha} Q_{\nu_\alpha \leftarrow \nu_\beta}, \quad Q_{\text{em}} = \sum_{\alpha} Q_{\text{em} \leftarrow \nu_\alpha}, \quad (2.31)$$

$$J_{\nu_\alpha} = J_{\nu_\alpha \leftarrow \text{em}} + \sum_{\beta \neq \alpha} J_{\nu_\alpha \leftarrow \nu_\beta}. \quad (2.32)$$

We note that in this approach, the self-interactions of neutrinos of flavour α do not play a role, even though in the physical world they can redistribute momenta.

The transfer rates close the system defined by eqs. (2.3)–(2.7). While slightly lengthier than the $m_e \rightarrow 0$ Maxwell-Boltzmann approximations in eq. (2.12), they are still compact, and more accurate and flexible than before. As described in sec. 8, we provide an easy-to-use code and tables based on the above procedure at [nudec_BSM_v2](#).

3. INCLUSION OF DYNAMICAL OSCILLATIONS IN THE MOMENTUM-AVERAGED APPROACH

It is possible to include dynamical neutrino oscillations in the momentum-averaged approach. Though the effect is not expected to be large in the SM [44, 45], it is worth checking its magnitude within our approach, as is can become relevant for several BSM scenarios, as will be discussed in more detail in Part II [63].

The system that we would like to solve is given by the Liouville equation,

$$(\partial_t - H q \partial_q) \varrho_\nu(t, \mathbf{q}) = -i[\mathcal{H}, \varrho_\nu(t, \mathbf{q})] + j[\varrho_\nu], \quad (3.1)$$

where the part $j[\varrho_\nu]$ accounts for the interaction rates [77]. In the absence of any asymmetry, the anti-neutrino density matrix, $\varrho_{\bar{\nu}}$, obeys the same evolution equation as ϱ_ν . Considering ultrarelativistic neutrinos, and omitting a part proportional to the unit matrix, the Hamiltonian \mathcal{H} is given in the flavour basis by

$$\mathcal{H} = U \frac{\Delta M^2}{2q} U^\dagger + \mathcal{V}, \quad (3.2)$$

where U is the PMNS matrix [78], $\Delta M^2 = \text{diag}(0, \Delta m_{21}^2, \Delta m_{31}^2)$ the neutrino mass matrix, and \mathcal{V} the matter potential [79]. For the neutrino mixing angles and masses, we insert the latest global three-neutrino fit [80],

$$(\sin^2 \theta_{12}, \sin^2 \theta_{23}, \sin^2 \theta_{13}) = (0.308, 0.470, 0.02215), \quad (3.3)$$

$$(\Delta m_{21}^2, \Delta m_{31}^2) = (7.49 \times 10^{-5} \text{ eV}^2, 2.514 \times 10^{-3} \text{ eV}^2), \quad (3.4)$$

assuming normal hierarchy for the neutrino masses. We neglect a possible CP-violating phase in the leptonic sector, as it has been shown to have a negligible impact on N_{eff} [68].

Following refs. [81, 82], the density matrix is generalized from eqs. (2.9) and (2.10) into

$$\varrho_\nu(t, \mathbf{q}) \equiv \frac{1}{e^{q/T_\nu} + 1} \times \mathcal{R}_\nu(t), \quad (3.5)$$

where \mathcal{R}_ν retains the matrix structure and is independent of the momentum q . The evolution equation for \mathcal{R}_ν can be obtained by integrating eq. (3.1) over \mathbf{q} ; an explicit derivation can be found in ref. [81].

At temperatures sufficiently below neutrino decoupling, $T_\nu \leq 1.5$ MeV, neutrino flavour oscillations become increasingly fast. This implies that in the mass basis, \mathcal{R}_ν converges to a diagonal matrix. Physical observables can then be extracted in the same way as done from the solution of a full Liouville equation, following eq. (C.7).

For the numerical calculations, we use a C++ code, inspired by the publicly available COFLASY-C code [82]. Instead of using various approximations as in ref. [81], we include the full neutrino-neutrino and neutrino-electron collision terms reported in ref. [45]. This allows us not only to include neutrino oscillations, but to have identical collision terms as in Fortepiano [69], and hence provide a fair comparison.

4. QED CORRECTIONS TO ENERGY DENSITY AND PRESSURE

Apart from the rates of energy and number density transfer between the QED and neutrino ensembles, an important ingredient for eqs. (2.6) and (2.7) is given by the QED energy density and pressure, ρ_{em} and p_{em} . The determination of these functions has a long history, with the neutrino decoupling codes usually making use of the expressions given in ref. [73]. They include QED corrections up to $\mathcal{O}(e^3)$, normally omitting a set of arguably small “logarithmic” corrections of $\mathcal{O}(e^2)$.

As a part of the current study, we have scrutinized the QED corrections to the energy density and pressure. Up to $\mathcal{O}(e^3)$, our results agree with ref. [73], however we find representations which are substantially simpler than reported there. Given that fewer special functions appear and unnecessary numerical cancellations can thereby be avoided, the simplified expressions can help to speed up the numerical evaluation. Our detailed results are given in appendix D.

We have also studied the influence of the terms of $\mathcal{O}(e^4)$ and $\mathcal{O}(e^5)$. These are fully known only in the high-temperature limit, $T_\gamma \gg m_e$. They are conceptually important in the sense that in that domain, they are the leading corrections yielding a trace anomaly, i.e. $\rho_{\text{em}} - 3p_{\text{em}} = \mathcal{O}(e^4 T_\gamma^4)$. With the help of renormalization group invariance, we have been able to extend parts of the results to any temperature.

To be concrete, in the massless limit, the pressure is often expressed as

$$p_{\text{em}} = \frac{\pi^2 T_\gamma^4}{45} \left[c_0 + e^2(\bar{\mu}) c_2 + e^3(\bar{\mu}) c_3 + e^4(\bar{\mu}) \left(\tilde{c}_4 \ln \frac{\bar{\mu}}{T_\gamma} + c_4 \right) + e^5(\bar{\mu}) \left(\tilde{c}_5 \ln \frac{\bar{\mu}}{T_\gamma} + c_5 \right) + \dots \right]. \quad (4.1)$$

Here $\bar{\mu}$ is the $\overline{\text{MS}}$ scheme renormalization scale; at this level of resolution, the running of e^2 needs to be taken into account (in contrast, m_e is defined as the “pole mass”, which does not run). At 1-loop order, which is sufficient for

our purposes, the running goes as

$$\bar{\mu} \frac{de^2(\bar{\mu})}{d\bar{\mu}} = \frac{e^4(\bar{\mu})}{6\pi^2} \Rightarrow e^2(\bar{\mu}) = \frac{6\pi^2}{\ln(\Lambda/\bar{\mu})}, \quad (4.2)$$

where Λ is an integration constant. When no argument is given, we assume $\bar{\mu} = m_e$, so that $e^2 \equiv e^2(\bar{\mu} = m_e) \approx 4\pi/137$.

As a physical quantity, the (temperature-dependent part of the) pressure must be independent of $\bar{\mu}$. This implies that

$$\bar{\mu} \frac{dp_{\text{em}}}{d\bar{\mu}} = 0 \stackrel{(4.1)}{\Rightarrow} \tilde{c}_4 = -\frac{c_2}{6\pi^2}, \quad \tilde{c}_5 = -\frac{c_3}{4\pi^2}. \quad (4.3)$$

These relations are also valid in the massive case, and allow to extract a part of the result in terms of the lower-order coefficients c_2 and c_3 .⁵ The results are reported in appendix D. In the end, the numerical effect that we find from these corrections is clearly below the accuracy of the momentum-averaged approach. The same is the case with the logarithmic corrections of $\mathcal{O}(e^2)$, though they grow in relative importance at low T_γ . As described in sec. 8, all corrections are included as tables (cf. table III) in `nudec_BSM_v2`, and for most of them we provide fast analytic representations (cf. appendix E).

5. PARAMETRIZATION OF THE UNIVERSE EXPANSION IN TERMS OF N_{eff} AND h_{eff}

The properties of the non-equilibrium neutrino ensembles, as determined by the solution of eqs. (2.3)–(2.7) or (3.1), dictate the expansion rate of the universe during the BBN and CMB epochs. Moreover, the overall amount of expansion that took place is relevant for the abundance of pre-existing cosmological relics, such as dark matter, baryon asymmetry, and primordial gravitational waves (cf. sec. 7). These two characteristics, instantaneous expansion rate and expansion accrued, can be characterized by the quantities that we call N_{eff} and h_{eff} , respectively.

If we consider the Hubble rate from eq. (2.7) at temperatures $T_m \ll T_\gamma \ll m_e$, where $T_m \sim \text{eV}$ denotes the moment of matter-radiation equality, the radiative QED corrections to ρ_{em} drop out, and we can write

$$\rho_t \equiv g_{*\rho} \frac{\pi^2}{30} T_\gamma^4 \quad \text{with} \quad g_{*\rho} \stackrel{T_m \ll T_\gamma \ll m_e}{\equiv} 2 \left[1 + \frac{7}{8} \left(\frac{4}{11} \right)^{4/3} N_{\text{eff}} \right]. \quad (5.1)$$

Therefore, N_{eff} parametrizes the Hubble rate at keV scale temperatures. Put another way,

$$N_{\text{eff}} \equiv \frac{8}{7} \left(\frac{11}{4} \right)^{4/3} \left(\frac{\rho_t - \rho_{\text{em}}}{\rho_{\text{em}}} \right) \Big|_{T_m \ll T_\gamma \ll m_e}. \quad (5.2)$$

In the Standard Model, and for the simplest case where one describes the neutrinos as a perfect fluid characterized by a single temperature, N_{eff} is given by

$$N_{\text{eff}}|_{\text{SM}} \approx 3 \left(\frac{11}{4} \right)^{4/3} \left(\frac{T_\nu}{T_\gamma} \right)^4. \quad (5.3)$$

However, knowing the Hubble rate at $T_\gamma \ll m_e$ does not provide complete information about the previous expansion history. We therefore also define another quantity, denoted by h_{eff} , which determines how the cosmological scale factor evolves from some initial time (a_{ini}) till today (a_0). Given that the influence of neutrino decoupling on this characteristic has received less attention than N_{eff} , let us provide some more background.

The text-book logic for determining the evolution of the scale factor goes via entropy conservation. *Assuming* thermal equilibrium, and combining Friedmann equations and thermodynamic identities, one finds that $sa^3 = \text{constant}$, where s denotes the entropy density (cf. the discussion below eq. (C.5)). Once neutrinos decouple, they are no longer in thermal equilibrium, and the logic needs to be rethought. However, one possibility is to *define* a non-equilibrium

⁵ As discussed below eq. (D.44), two coefficients remain in eq. (4.1), denoted by c_4 and c_5 , which are only known in the massless limit.

Given that only the massless values are known, these coefficients do not go away at low $T_\gamma \ll m_e$, even though their mass-dependent generalizations would do so. However, this has no practical influence.

entropy such that it is effectively conserved, writing

$$h_* \times (aT_\gamma)^3 \equiv \text{constant} , \quad s \equiv h_* \frac{2\pi^2 T_\gamma^3}{45} . \quad (5.4)$$

Then the evolution of the scale factor is given by

$$\frac{a_{\text{ini}}}{a_0} \stackrel{(5.4)}{=} \left(\frac{h_{*,0}}{h_{*,\text{ini}}} \right)^{1/3} \frac{T_{\gamma,0}}{T_{\gamma,\text{ini}}} . \quad (5.5)$$

In terms of the variable z determined via eq. (2.8), we can compute $h_{*,0}$ as

$$h_{\text{eff}} \equiv h_{*,0} \stackrel{(2.8)}{\underset{(5.5)}{=}} \frac{h_{*,\text{ini}}}{z_0^3} . \quad (5.6)$$

After neutrino decoupling has completed, the photon temperature redshifts with the universe expansion, so that eq. (5.6) becomes constant with respect to $T_{\gamma,0}$. Therefore, we may evaluate h_{eff} at the final moment of our evolution, $T_{\gamma,0} \rightarrow T_{\gamma,\text{fin}}$. In practice, we choose $T_{\gamma,\text{fin}} \approx 0.01$ MeV. To ensure that particles like muons and pions, which we do not include our equation of state, matter very little, a suitable initial moment is $T_{\gamma,\text{ini}} = 10$ MeV. From eq. (D.15), we then obtain $h_{*,\text{ini}} = 10.736$. With this initial value and a solution of eq. (2.8), the value of h_{eff} follows from eq. (5.6).

It is appropriate to stress that the definition of a non-equilibrium entropy coefficient via eq. (5.6) is *not* unique. Indeed there is another frequently used definition in the context of neutrino decoupling, which we recall in appendix C 1; to make the distinction clear, we refer to the latter with g_{*s} .

6. MAIN RESULTS AND THEIR COMPARISON WITH THE LIOUVILLE EQUATION

As discussed above, in the momentum-averaged approach the neutrino decoupling process is described by simple ordinary differential equations for the electromagnetic temperature (eq. (2.6)), as well as the neutrino temperature(s) and effective chemical potentials (eqs. (2.3)), all linked via the Hubble rate (eq. (2.7)). This system of equations is parametrized by the neutrino interaction rates (sec. 2B) and by the energy density and pressure of the QED plasma (sec. 4). With these ingredients, we obtain a fast solution ($t_{\text{CPU}} \lesssim 1$ s), which can be compared with the solution of the momentum-dependent system of $\mathcal{O}(100)$ coupled stiff integro-differential equations obtained with Fortepiano [69]. Here we summarize the results of the comparison, relegating the technical details to appendix C.

Table I shows the main results of our study. We tabulate the effective number of relativistic neutrinos, N_{eff} (cf. eq. (5.2)); the corresponding total number of degrees of freedom contributing to the energy density, $g_{*\rho}$ (cf. eq. (5.1)); a definition of entropy degrees of freedom obtained from kinetic theory, g_{*s} (cf. eq. (C.10)); a definition of entropy degrees of freedom parametrizing the expansion of the universe, h_{eff} (cf. eq. (5.6)); and a measure of the energy density that neutrinos carry in the late universe, $\sum m_\nu / [\Omega_\nu h^2 \text{ eV}]$ (cf. eq. (C.12)). In our results, the part with *no oscillations* means that we treat ν_e and $\nu_{\mu/\tau}$ as separate fluids, while for the results *with oscillations*, the approach of eq. (2.9) assumes the oscillations to be so fast that all flavours are described by a joint averaged fluid.

Accuracy of the approach for Standard Model characteristics. — The comparison between our results and those of Fortepiano indicates that the differences of all cosmological parameters are less than 0.05% in the Standard Model, and can be reduced to below 0.03% if chemical potentials are included in the neutrino distribution functions. If oscillations are omitted on both sides, chemical potentials increase the accuracy to 0.01%. This is rather remarkable in view of the simplicity of our approach. Our N_{eff} agrees very well with the value $N_{\text{eff}} \simeq 3.044$, obtained by refs. [67–69]. We note that the numerical convergence of these references is 0.006%, which means we have agreement up to numerical errors in some cases. From table I, we see that allowing for neutrino chemical potentials increases the precision most significantly for $\Omega_\nu h^2$, as chemical potentials affect more strongly the number density of neutrinos.

As for the entropy density, we find a remarkable numerical agreement between the two definitions we have considered, g_{*s} and h_{eff} (cf. table I). The final value, $h_{\text{eff}} \approx 3.930$, differs noticeably from that implied by the latest PDG edition [78].⁶ We believe that this number is worth taking into account, as the improvement is comparable to the

⁶ When citing a value for the current entropy density of the universe, which is regularly used in the sense of eq. (5.5), ref. [78] cites

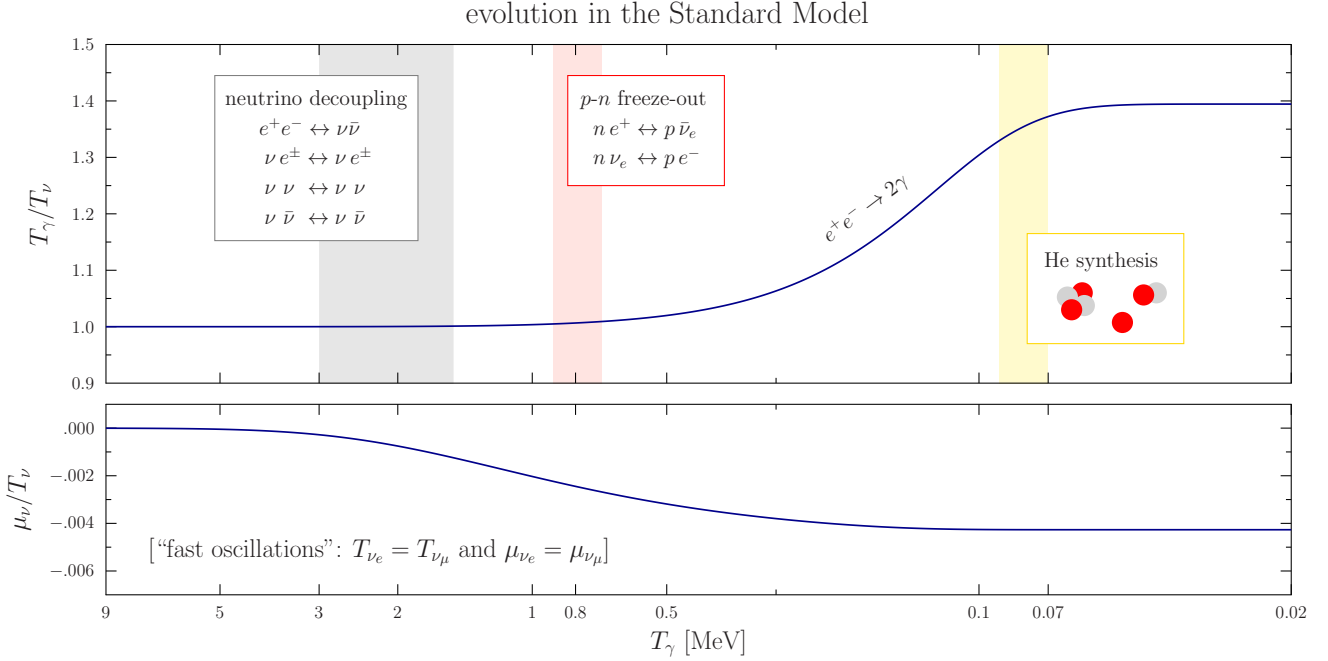


FIG. 2. Evolution of the neutrino temperature and (effective) chemical potential in the Standard Model, as a function of T_γ . In this plot, the “fast oscillation” case from eq. (2.9) is assumed, see table I for the corresponding cosmological parameters. The increase in the ratio T_γ/T_ν with time is chiefly due to heating from $e^+e^- \rightarrow 2\gamma$, while the deviation in the parameter μ_ν from zero tracks the spectral distortions in the neutrino momentum distribution.

current error on e.g. the dark matter or baryon asymmetry in the universe, and has an impact on the corresponding theoretical computations.

In fig. 2 we show the thermodynamic evolution as a function of T_γ for the case where the entire neutrino fluid is characterized by a common temperature and effective chemical potential. The evolution of T_γ/T_ν illustrates the usual behaviour: at high temperatures $T_\gamma \gtrsim 3$ MeV, photons and neutrinos remain in tight thermal equilibrium, followed by subsequent relative photon heating due to $e^+e^- \rightarrow 2\gamma$ annihilations. In the lower panel, we show μ_ν/T_ν , highlighting when the spectral distortions to the neutrino distribution function develop.

The differential neutrino distribution functions are shown in fig. 3. The determination of spectral distortions is a key goal of the Liouville approach (cf., e.g., fig. 3 of ref. [67] or fig. 4 of ref. [68]), however usually the comparison is against a Fermi distribution without a chemical potential. Given that neutrino temperatures and chemical potentials are ingredients of our momentum-averaged approach, it is natural to ask how large the distortions are relative to this generalized reference point. Our comparison shows that the differences are smaller than $\lesssim 0.03\%$. This is in concordance with the results of ref. [83], which highlight that a modified temperature and chemical potential can account for most of, but not all, the spectral distortions. In any case, from our approach we conclude that the spectral distortions of the Cosmic Neutrino Background are at the $\lesssim 0.03\%$ level. In the right panel of fig. 3, we also show the comparison directly with the distribution function, observing differences of up to 0.1% in the infrared domain $q_\nu/T_\nu \lesssim 2.0$. However, this part is phase-space suppressed in the integrated number and energy densities.

Treatment of neutrino oscillations. — In table I, we include results from the approach described in sec. 3 that accounts for dynamical neutrino oscillations. We see that the agreement between that approach and Fortepiano is better than 0.012% for any cosmological parameter, and the same holds for the neutrino distribution function. While this procedure is significantly more involved than just tracking temperatures and chemical potentials, the agreement is important, as it will allow us to scrutinize the impact of neutrino oscillations in BSM settings [63].

Higher-order QED effects. — Although not shown in table I, we find the impact of the $\mathcal{O}(e^4)$ and $\mathcal{O}(e^5)$ corrections to the thermodynamics of the QED plasma to be quite small. In particular, they shift N_{eff} by $\lesssim 2 \times 10^{-5}$ as compared

$h_{*,0} = 43/11 \approx 3.91$, which originates from essentially the same estimate as the naive $N_{\text{eff}} = 3.0$.

Neutrino Decoupling in the Standard Model: key parameters and observables						
case/parameter	N_{eff}	$g_{*\rho}$	g_{*s}	h_{eff}	$\sum m_\nu / [\Omega_\nu h^2 \text{ eV}]$	
<i>no oscillations:</i>						
Fortepiano [69]	3.0435	3.3824	3.9298	3.9296	93.129	
this work $\mu_\nu = 0$	3.0443 [0.028%]	3.3828 [0.012%]	3.9302 [0.011%]	3.9301 [0.019%]	93.035	[-0.10%]
this work $\mu_\nu \neq 0$	3.0437 [0.006%]	3.3825 [0.003%]	3.9299 [0.002%]	3.9298 [0.010%]	93.127	[-0.002%]
<i>with oscillations:</i>						
Fortepiano [69]	3.0439	3.3826	3.9302	3.9298	93.119	
this work $\mu_\nu = 0$	3.0453 [0.044%]	3.3832 [0.018%]	3.9307 [0.011%]	3.9306 [0.025%]	93.013	[-0.11%]
this work $\mu_\nu \neq 0$	3.0446 [0.020%]	3.3829 [0.009%]	3.9303 [0.003%]	3.9302 [0.020%]	93.108	[-0.01%]
this work sec. 3	3.0443 [0.012%]	3.3827 [0.004%]	3.9302 [-0.001%]	3.9301 [0.008%]	93.116	[-0.003%]

TABLE I. Standard Model results as obtained in this work (`nudec_BSM_v2`) by solving for the time evolution of T_γ , T_{ν_e} , T_{ν_μ} , effective neutrino chemical potentials, and the scale factor, a . We compare our results in terms of N_{eff} (cf. eq. (5.2)), $g_{*\rho}$ (cf. eq. (5.1)), g_{*s} (cf. eq. (C.10)), h_{eff} (cf. eq. (5.6)) and $\sum m_\nu / \Omega_\nu h^2$ (cf. eq. (C.12)) against the Liouville solution from Fortepiano with high accuracy settings [69]. The results include the QED equation of state including $\mathcal{O}(e^3)$, ignoring logarithmic corrections at $\mathcal{O}(e^2)$, and employing the low-energy constants from eq. (A.2). “No oscillations” and “with oscillations” refer to the assumptions in eq. (2.9), or to the more general framework of sec. 3. Sec. 3 with $\Delta M^2 \rightarrow 0$ in eq. (3.2) leads to essentially the same result as “no oscillations” with $\mu_\nu \neq 0$. The neutrino masses and mixing angles are fixed according to eq. (3.4).

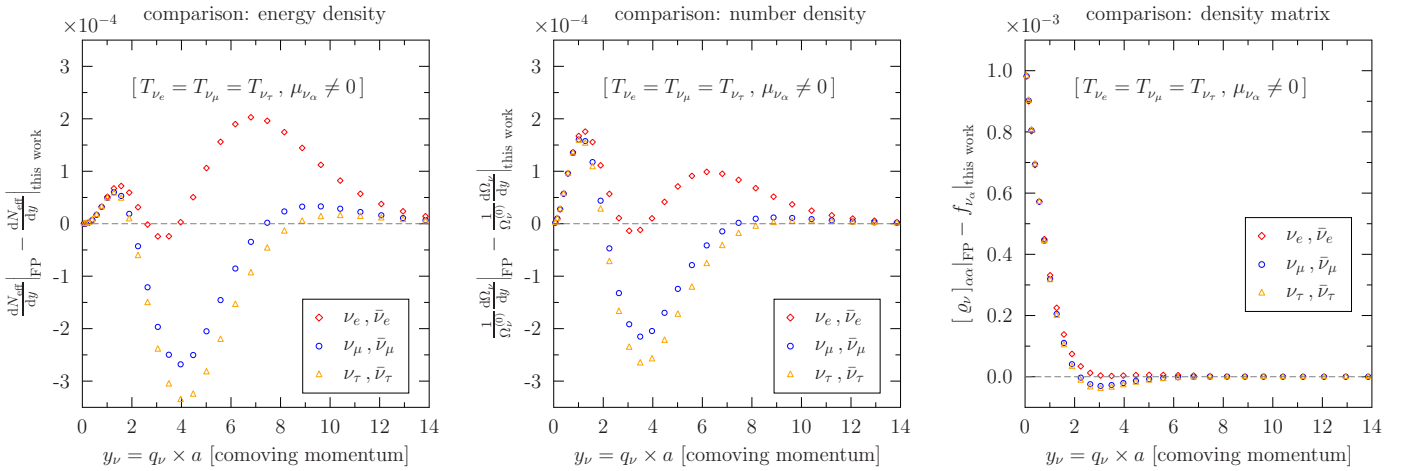


FIG. 3. The difference of the (weighted) neutrino distribution function between our results and Fortepiano [69]. The panels display the same information in different ways, moving from left to right: the differential energy density ($dN_{\text{eff}} \equiv \frac{120}{7\pi^4} (\frac{11}{4})^{4/3} \frac{y^3}{z^4} \frac{dy}{dy}$ f_{ν_α} , cf. eqs. (C.13) and (5.2)); the differential number density ($d\Omega_\nu / \Omega_\nu^{(0)} \equiv \frac{2}{3\zeta(3)} \frac{11}{4} \frac{y^2}{z^3} \frac{dy}{dy} f_{\nu_\alpha}$, cf. eqs. (C.12), (C.14), and table V); and the momentum distribution itself. On the x -axis, a is normalized to $1/T_\nu$ at the initial temperature, i.e. $a \equiv a/(aT_\nu)_{\text{ini}}$. In the nomenclature of table I, we show the comparison *with oscillations*, having included the neutrino chemical potentials. In the left and middle panels, the spectral distortions are $\lesssim 0.03\%$ across comoving neutrino momenta.

with the result considering corrections up to $\mathcal{O}(e^3)$. This shift is actually somewhat smaller than the impact of the logarithmic $\mathcal{O}(e^2)$ contribution, which shifts N_{eff} by $\lesssim 3 \times 10^{-5}$, and which is also not included by default in Fortepiano. Given their small numerical impact, we conclude that these corrections can be neglected.

On the accuracy of the collision terms. — We note that we have performed all calculations for table I using the linear-response transfer rates shown in fig. 1. However, by solving the neutrino and QED plasma evolution using at each time step the full collision terms (integrated over three dimensions), we obtain the very same results for N_{eff} . This demonstrates the accuracy of our linear-response collision terms, and makes us confident that they will perform well also beyond the Standard Model.

7. OUTLINE OF BSM EXTENSIONS

The main motivation for the momentum-averaged approach is that it can straightforwardly incorporate other subsystems on top of the QED and neutrino ones. For concreteness, denoting such a species by x , eqs. (2.1) and (2.2) would then be supplemented by

$$\dot{\rho}_x + 3H(\rho_x + p_x) = Q_x, \quad \dot{n}_x + 3Hn_x = J_x. \quad (7.1)$$

The transfer rates include a contribution from the other ensembles, e.g. $Q_x = \sum_i Q_{x \leftarrow i}$, with $i \in \{\text{em}, \nu_e, \nu_\mu, \nu_\tau\}$. Vice versa, the previous energy transfer rates, Q_i , need to be supplemented by the energy insertions from x , $Q_{i \leftarrow x}$, as dictated by detailed balance. In addition, the contribution from x needs to be added to the Hubble rate, in eq. (2.7), and to the initial value of h_* , in eq. (D.15).

In many BSM models, $Q_x = J_x = 0$ during the decoupling period, implying that x is *not* in equilibrium with the QED plasma. Then the dynamics of x is easy to incorporate. For instance, for typical cold dark matter candidates, with $p_x \ll \rho_x$, eq. (7.1) amounts to $\dot{\rho}_x + 3H\rho_x \approx 0$, with the solution

$$\rho_{x,0} \stackrel{Q_x \approx 0}{\underset{p_x \ll \rho_x}{\approx}} \rho_{x,\text{ini}} \left(\frac{a_{\text{ini}}}{a_0} \right)^3 \stackrel{(5.4)}{=} \rho_{x,\text{ini}} \frac{h_{\text{eff}}}{h_{*,\text{ini}}} \left(\frac{T_{\gamma,0}}{T_{\gamma,\text{ini}}} \right)^3. \quad (7.2)$$

Similarly, for dark radiation, such as gravitational waves, with $p_x \approx \rho_x/3$, the initial energy density just gets diluted as $(a_{\text{ini}}/a_{\text{fin}})^4$, and their contribution to N_{eff} can subsequently be estimated from eq. (5.1).

The non-trivial case is if $Q_x \neq 0$, or if x contributes significantly to H during neutrino decoupling. Such situations are straightforward to add to our framework, however the details and results are model-dependent. We return to well-motivated examples in ref. [63].

8. NOTES ON NUMERICAL CODES AND DATA TABLES

The **Mathematica** and **python** packages implementing our framework are available as `nudec_BSM_v2`. In addition to the numerical integrators, the repository includes data tables for the functions plotted in fig. 1, and an efficient evaluator of the QED equation of state discussed in sec. 4. The parameters are chosen as specified in appendix A, and the initial and final temperatures are by default set to

$$T_{\gamma,\text{ini}} = 10 \text{ MeV}, \quad T_{\gamma,\text{fin}} \approx 0.01 \text{ MeV}. \quad (8.1)$$

The main **Mathematica** and **python** module files are stored in the subdirectory `BasicModules_source/`. For the **python** implementation, some minimal examples of how to run the code are provided in `test.py` and `nudec.ipynb`. For the **Mathematica** implementation, several different Standard Model scenarios are provided in the notebook `Neff_SM.nb`. When the test programs are run, they produce output files containing the solution. For reference, the results obtained with our default parameters can be found in the subdirectory `SM_results/`.

The pre-computed input tables are in a subdirectory called `BasicModules_data/`. They contain the rate coefficients defined in sec. 2B, as well as the QED pressure and its first and second temperature derivatives. For reference, we show examples of the rate coefficients in table II, and examples of the QED pressure in table III. We also remark that, apart from downloading the QED pressure from tables, the code contains an option for its fast evaluation in terms of Bessel functions, as explained in appendix E.

The **Mathematica** and **python** codes have identical modular structures, with the top layer solving the differential equations given in eqs. (2.3)–(2.7). It is straightforward to complement this system with further equations, as outlined in sec. 7, or to modify the input that enters the Standard Model solver (notably the rate coefficients, the QED equation of state, or the fundamental constants that we treat as fixed parameters).

m_e/T_γ	f_{a1}	f_{a2}	f_{a3}	f_{a4}	f_{s1}	f_{s2}	f_{s3}	f_{s4}	f_{n1}	f_{n2}	f_{n3}	f_{n4}
0.0	0.884	0.0	0.0318	0.0	0.829	0.0	0.0	0.0	0.852	0.0	0.041	0.0
\vdots	\vdots											
1.0	0.830	0.104	0.0428	-0.0165	0.722	-0.0379	0.0	0.0	0.787	0.121	0.0553	-0.0179
\vdots	\vdots											

TABLE II. Examples of the rate coefficients shown in fig. 1, as they appear in the data file `rate_coefficients_neutrinos.dat` that is available at `nudec_BSM_v2`.

T_γ [MeV]	$p_{\text{em}}^{(0)}$ [MeV 4]	$p_{\text{em}}^{(2) \text{ ln}}$ [MeV 4]	$p_{\text{em}}^{(2) \text{ ln}}$ [MeV 4]	$p_{\text{em}}^{(3)}$ [MeV 4]	$p_{\text{em}}^{(4)}$ [MeV 4]	$p_{\text{em}}^{(5)}$ [MeV 4]
\vdots	\vdots					
1.0	$+5.83 \times 10^{-1}$	-1.33×10^{-3}	$+1.77 \times 10^{-5}$	$+1.34 \times 10^{-4}$	-4.33×10^{-6}	-1.81×10^{-7}
\vdots	\vdots					
10.0	$+6.03 \times 10^{+3}$	$-1.59 \times 10^{+1}$	$+3.04 \times 10^{-3}$	$+1.42 \times 10^{+0}$	-1.02×10^{-1}	$+5.89 \times 10^{-3}$
\vdots	\vdots					

TABLE III. Examples of contributions of various orders to the QED pressure, as they appear in the data file `QED_p_int.dat` that is available at `nudec_BSM_v2`. We have here used $m_e = 0.51099895$ MeV and $\alpha_{\text{em}}(\bar{\mu} = m_e) = 1/137.035999084$. We supply similar tabulations for $\partial_{T_\gamma} p$ and $\partial_{T_\gamma}^2 p$ in the files `QED_dp_dT_int.dat` and `QED_d2p_dT2_int.dat`, respectively.

9. CONCLUSIONS

The main goal of this study has been to significantly improve on the momentum-averaged approach to solve for neutrino decoupling, and thereby to accurately determine cosmological parameters like N_{eff} and h_{eff} , see eqs. (5.1) and (5.6). In this context, direct outputs of our analysis are:

1. Refined but still compact linear-response representations of energy and number density transfer rates that take into account all relevant neutrino-electron and neutrino-neutrino interactions (sec. 2). We have validated the new representations by solving for neutrino decoupling in the Standard Model both with them, and with the full leading-order rates, finding identical results.
2. An investigation of corrections to the QED energy density and pressure at $\mathcal{O}(e^4)$ and $\mathcal{O}(e^5)$, showing that these yield numerically small contributions to N_{eff} and h_{eff} (sec. 4).
3. Verification that the accuracy of the momentum-averaged approach as compared with the Liouville equation is better than 0.04% for any integrated cosmological parameter in the Standard Model (sec. 6). Once we include dynamical neutrino oscillations, the agreement is close to the numerical precision level.
4. Determination of spectral distortions of the Cosmic Neutrino Background in the Standard Model, showing that compared with a distribution function containing an effective chemical potential, and including a phase-space factor as it appears in the number or energy density, they are $\lesssim 0.03\%$ for all comoving momenta (sec. 6).
5. Tabulation of key cosmological parameters for the Standard Model as a function of the photon temperature. We have also carefully defined and computed the entropy-related parameter $h_{\text{eff}} = 3.930$, improving upon the PDG value, which leads to $\sim 1\%$ shifts on primordial relic density abundances of dark matter or baryon asymmetry.

While we have improved upon many aspects of the momentum-averaged approach to solve for neutrino decoupling, it remains simple, numerically tractable, and computationally efficient. The corresponding `Mathematica` and `python` packages can be found at [GitHub](#) under the name `nudec_BSM_v2` (see sec. 8 for a short description). An important aspect is that as described in appendix E, we have been able to speed up the calculations by a factor of ~ 10 , making the codes suitable for fast cosmological inferences. Critically, the packages are portable and can easily be linked with

BBN codes. Given that the framework is general, it can also be employed for other thermodynamic processes in the early universe (e.g. involving dark sectors).

While we have focussed on the Standard Model in this paper, a key advantage of the approach, given its flexibility, is for studying BSM physics affecting neutrino decoupling. In fact, the present release already incorporates the possibility to explore the consequences of time-varying fundamental constants, such as m_e , s_W^2 , G_F , G_N , or α_{em} . Given the successful calibration of the accuracy of the momentum-averaged approach within the Standard Model, we will soon provide detailed investigations of well-motivated BSM extensions [63].

Acknowledgments

We thank Cara Giovanetti for helpful feedback about the implementation of our code in a BBN setup. M.E. and S.S. are grateful to Valerie Domcke and Mario Fernandez Navarro for their contribution to the development of neutrino oscillations in the momentum-averaged approach for neutrino decoupling. We acknowledge support from the DOE Topical Collaboration “Nuclear Theory for New Physics,” award No. DE-SC0023663. S.S. is supported by the US Department of Energy Office and by the Laboratory Directed Research and Development (LDRD) program of Los Alamos National Laboratory under project numbers 20230047DR and 20250164ER. Los Alamos National Laboratory is operated by Triad National Security, LLC, for the National Nuclear Security Administration of the U.S. Department of Energy (Contract No. 89233218CNA000001). G.J. is funded by the Agence Nationale de la Recherche (France), under grant ANR-22-CE31-0018 (AUTOTHERM).

Appendices

These appendices complement the main text by providing details aimed at practitioners. In summary:

- A. We specify our choices for the low-energy neutrino-electron interaction constants as well as the calculation of the relevant matrix element.
- B. We show how the f functions in eqs. (2.19)–(2.21) can be matched onto the general linear-response coefficients from eqs. (2.17) and (2.18).
- C. We provide definitions of key cosmological parameters and present a detailed comparison between our results and those obtained by solving the Liouville equation in the Standard Model.
- D. We present the calculation of the equation of state of the electromagnetic plasma up to $\mathcal{O}(e^5)$. We provide more compact expressions for the contributions up to $\mathcal{O}(e^3)$ than those in ref. [73]. The $\mathcal{O}(e^4)$ and $\mathcal{O}(e^5)$ contributions are new, but they turn out to be numerically negligible.
- E. We show how to expand various integrals over the thermal distribution functions as series in Bessel functions, or as polylogarithms. The corresponding speed-up in the code is a factor of ~ 10 . All of these functions are defined in `Mathematica` and `python` at [nudec_BSM_v2](#).

Appendix A: Couplings and matrix elements squared

The rate coefficients playing a role in the Standard Model originate from a Fermi vertex, which after a Fierz transformation can be expressed as

$$\begin{aligned} \mathcal{L}_I &\supset -2\sqrt{2}G_F \bar{\nu}_\alpha \gamma_\mu a_L \nu_\alpha \\ &\times \bar{\ell}_e \gamma^\mu \left\{ [\delta_{\alpha,e} g_{eR} + (1 - \delta_{\alpha,e}) g_{\mu R}] a_R + [\delta_{\alpha,e} g_{eL} + (1 - \delta_{\alpha,e}) g_{\mu L}] a_L \right\} \ell_e . \end{aligned} \quad (\text{A.1})$$

Here α is a flavour index, $a_L \equiv (1 - \gamma_5)/2$, $a_R \equiv (1 + \gamma_5)/2$, and $G_F = 1.1663787 \times 10^{-5} \text{ GeV}^{-2}$ is the Fermi coupling. For the Wilson coefficients we employ the values [84]

$$g_{eL} = 0.727, \quad g_{eR} = 0.233, \quad g_{\mu L} = -0.273, \quad g_{\mu R} = 0.233 , \quad (\text{A.2})$$

and for the QED parameters $m_e = 0.51099895 \text{ MeV}$ and $\alpha_{\text{em}} = e^2/(4\pi) = 1/137.035999084$ as in Fortepiano.

The vertex in eq. (A.1) gives rise to pair creation, pair annihilation, and scattering processes. The corresponding amplitudes can be obtained by crossing relations from each other, so it is sufficient to choose one example, say

$$\nu_e(\mathbf{k}_1, \sigma_1) + \bar{\nu}_e(\mathbf{k}_2, \sigma_2) \rightarrow \ell_e(\mathbf{p}_1, \tau_1) + \bar{\ell}_e(\mathbf{p}_2, \tau_2) , \quad (\text{A.3})$$

where σ_i , τ_i are spin indices, and we work in the flavour basis. The matrix element can be written as

$$\mathcal{M} = (\text{phase}) 2\sqrt{2} G_F \bar{v}(\mathbf{k}_2, \sigma_2) \gamma_\mu a_L u(\mathbf{k}_1, \sigma_1) \bar{u}(\mathbf{p}_1, \tau_1) \gamma^\mu (g_{eR} a_R + g_{eL} a_L) v(\mathbf{p}_2, \tau_2) , \quad (\text{A.4})$$

where u and v are the usual Dirac spinors. The matrix element squared reads

$$\begin{aligned} |\mathcal{M}|^2 &= 8G_F^2 \bar{v}(\mathbf{k}_2, \sigma_2) \gamma_\mu a_L u(\mathbf{k}_1, \sigma_1) \bar{u}(\mathbf{k}_1, \sigma_1) \gamma_\nu a_L v(\mathbf{k}_2, \sigma_2) \\ &\times \bar{u}(\mathbf{p}_1, \tau_1) \gamma^\mu (g_{eR} a_R + g_{eL} a_L) v(\mathbf{p}_2, \tau_2) \bar{v}(\mathbf{p}_2, \tau_2) \gamma^\nu (g_{eR} a_R + g_{eL} a_L) u(\mathbf{p}_1, \tau_1) . \end{aligned} \quad (\text{A.5})$$

We can sum over spins, and insert completeness relations. In addition, we can symmetrize the result in $\mathbf{p}_1 \leftrightarrow \mathbf{p}_2$, given that we assume the QED plasma to be charge-symmetric (in the case of scatterings, this means that neutrinos

can scatter both off electrons and off positrons). All in all this yields

$$\sum_{\sigma_i, \tau_i} |\mathcal{M}|^2 \xrightarrow{\mathbf{p}_1 \leftrightarrow \mathbf{p}_2} 16G_F^2 \left\{ (g_{eR}^2 + g_{eL}^2) [(t - m_e^2)^2 + (u - m_e^2)^2] + 4g_{eL}g_{eR}m_e^2s \right\}, \quad (\text{A.6})$$

where s, t, u are the usual Mandelstam variables. All other matrix elements squared can be obtained from eq. (A.6) by crossings.

Appendix B: Parametrization of the rate coefficients

We specify here how the functions defined in eqs. (2.19)–(2.21) can be matched onto the coefficients from eqs. (2.17) and (2.18), so that the full electron mass dependence is retained in the linear response regime. All 12 functions can be related to the derivatives in eqs. (2.17)–(2.18), by expanding the expressions for small ϵ_T and ϵ_μ . To be concrete,

$$f_{a1} = \frac{-1}{1152} \widehat{Q}_1^{(1,0)} \Big|_{\text{gain-loss}}, \quad f_{a2} = \frac{-1}{1152} \widehat{Q}_2^{(1,0)} \Big|_{\text{gain-loss}}, \quad (\text{B.1})$$

$$f_{a3} = f_{a1} + \frac{1}{256} \widehat{Q}_1^{(0,1)} \Big|_{\text{gain-loss}}, \quad f_{a4} = f_{a2} + \frac{1}{256} \widehat{Q}_2^{(0,1)} \Big|_{\text{gain-loss}}, \quad (\text{B.2})$$

$$f_{s1} = \frac{-1}{224} \widehat{Q}_1^{(1,0)} \Big|_{\text{scattering}}, \quad f_{s2} = \frac{-1}{224} \widehat{Q}_2^{(1,0)} \Big|_{\text{scattering}}, \quad (\text{B.3})$$

$$f_{s3} = \frac{1}{224} \widehat{Q}_1^{(0,1)} \Big|_{\text{scattering}}, \quad f_{s4} = \frac{1}{224} \widehat{Q}_2^{(0,1)} \Big|_{\text{scattering}}, \quad (\text{B.4})$$

$$f_{n1} = \frac{-1}{256} \widehat{J}_1^{(1,0)} \Big|_{\text{gain-loss}}, \quad f_{n2} = \frac{-1}{256} \widehat{J}_2^{(1,0)} \Big|_{\text{gain-loss}}, \quad (\text{B.5})$$

$$f_{n3} = f_{n1} + \frac{1}{64} \widehat{J}_1^{(0,1)} \Big|_{\text{gain-loss}}, \quad f_{n4} = f_{n2} + \frac{1}{64} \widehat{J}_2^{(0,1)} \Big|_{\text{gain-loss}}. \quad (\text{B.6})$$

The relevant partial derivatives can be evaluated numerically, making use of the spectral functions from appendix B of ref. [76] and implementing neutrino chemical potentials according to appendix A.3 of ref. [60].

Several of these functions have known limits for $m_e \rightarrow 0$. First, if electrons are taken to be massless, then f_{x2} and f_{x4} (for $x = a, s, n$) all vanish. And second, in this same limit, $f_{a1}(0) = f_a^{\text{FD}}$, $f_{s1}(0) = f_s^{\text{FD}}$, and $f_{n1}(0) = f_n^{\text{FD}}$, where the functions f_x^{FD} were implemented in ref. [60] to account for Fermi-Dirac statistics.

Appendix C: Comparison in the Standard Model: momentum-averaged vs. Liouville solution

In this appendix we compare the results for neutrino decoupling between the momentum-averaged equations from sec. 2A, and the Liouville equation as calculated in Fortepiano [69]. In order to output a fair comparison we consider the same set of low-energy constants describing neutrino-electron interactions, specified in eq. (A.2), and keep terms up to $\mathcal{O}(e^3)$ in the QED energy density and pressure (ignoring a logarithmic term of $\mathcal{O}(e^2)$). Before proceeding to the comparison, we need to state how the relevant parameters are defined and how they can be extracted.

1. On different definitions of entropy density

While we have given one definition of entropy density, parametrized by the coefficient h_* , in eq. (5.4), let us start by elaborating on another definition. For a non-interacting fermionic fluid with two degrees of freedom, which is not in thermal equilibrium, an entropy density can be defined as (cf., e.g., [85, eq. (3.55)] or [77, eq. (3.10)])

$$s_\nu \equiv -2 \int_{\mathbf{q}} [f_\nu \ln f_\nu + (1 - f_\nu) \ln(1 - f_\nu)]. \quad (\text{C.1})$$

Making use of the pressure from eq. (2.11), and inserting the ansatz from eq. (2.10), we get

$$s_\nu = \frac{p_\nu}{T_\nu} - 2 \int_{\mathbf{q}} f_\nu \ln \frac{f_\nu}{1-f_\nu} \stackrel{(2.10)}{\underset{(2.11)}{\equiv}} \frac{\rho_\nu + p_\nu - \mu_\nu n_\nu}{T_\nu}. \quad (\text{C.2})$$

Summing over the photons and neutrino flavours, we define the coefficient g_{*s} via

$$\sum_i s_i \equiv \sum_i \frac{\rho_i + p_i - \mu_i n_i}{T_i} \stackrel{T_m \ll T_\gamma \ll m_e}{\underset{\mu_\gamma = 0}{\equiv}} g_{*s} \frac{2\pi^2}{45} T_\gamma^3, \quad (\text{C.3})$$

where $T_m \sim \text{eV}$ is the moment of matter-radiation equality. Looking at changes of eq. (C.1), we get

$$ds_\nu \stackrel{(C.1)}{=} -2 \int_{\mathbf{q}} [df_\nu \ln f_\nu + df_\nu - df_\nu \ln(1-f_\nu) - df_\nu] = -2 \int_{\mathbf{q}} df_\nu \ln \frac{f_\nu}{1-f_\nu} \stackrel{(2.10)}{\underset{(2.11)}{\equiv}} \frac{d\rho_\nu - \mu_\nu dn_\nu}{T_\nu}, \quad (\text{C.4})$$

which has the form of the first law of thermodynamics,

$$d\rho_\nu = T_\nu ds_\nu + \mu_\nu dn_\nu. \quad (\text{C.5})$$

Inserting $\rho_i + p_i = T_i s_i + \mu_i n_i$ (cf. eq. (C.3)) and eq. (C.5) into overall energy conservation, eq. (2.1), we find

$$\sum_i [T_i \partial_t(s_i a^3) + \mu_i \partial_t(n_i a^3)] = 0. \quad (\text{C.6})$$

If we had a unique temperature ($T_i = T \forall i$), unique chemical potentials ($\mu_i = \mu \forall i$), and conserved particle numbers ($\partial_t(\sum_i n_i a^3) = 0$), the overall entropy defined in accordance with eq. (C.3), $\sum_i s_i a^3$, would be conserved. As none of these conditions is met, this is not guaranteed to be the case. Therefore, g_{*s} could differ from h_* , with the latter having been defined so as to make the entropy-like quantity in eq. (5.4) a constant of motion.

2. Extraction of cosmological parameters from a neutrino density matrix

When solving the Liouville equation (cf. eq. (3.1)), whether without approximation on a momentum grid, or via a momentum-averaged ansatz as explained in sec. 3, the output quantity is the neutrino density matrix, ϱ_ν . The neutrino phase space distributions can be obtained by reading out the diagonal components (cf. eq. (2.9)),

$$f_{\nu_\alpha}(t, q) \equiv [\varrho_\nu(t, \mathbf{q})]_{\alpha\alpha}, \quad \alpha \in \{e, \mu, \tau\}. \quad (\text{C.7})$$

Given the phase space distributions, energy density, number density, and pressure can be determined according to eq. (2.11). From the energy density, we then obtain $g_{*\rho}$ and N_{eff} in accordance with eqs. (5.1) and (5.2), respectively. The entropy-related coefficient h_{eff} can be obtained from eq. (5.6).

The entropy defined according to eq. (C.1) can similarly be obtained from f_{ν_α} . To be quite concrete, we remark that Fortepiano employs the notation

$$x \equiv am_e, \quad y \equiv aq, \quad z \equiv aT_\gamma, \quad (\text{C.8})$$

where the units of the scale factor have been chosen so that $a = 1/T_\nu = 1/T_\gamma$ at the initial time, i.e. $a \equiv a/(aT_\gamma)_{\text{ini}}$ (we show this explicitly in eqs. (2.8) and (D.4)). The time variable is effectively x , while y represents the comoving momentum. With this in mind, we can write g_{*s} as

$$g_{*s} \stackrel{(C.1)}{\underset{(C.3)}{\equiv}} 2 - \frac{45}{2\pi^2} \frac{2}{2\pi^2} \frac{1}{z^3} \sum_\alpha \int_0^\infty dy y^2 [f_{\nu_\alpha} \ln f_{\nu_\alpha} + (1-f_{\nu_\alpha}) \ln(1-f_{\nu_\alpha})] \quad [\text{non-thermal distributions}], \quad (\text{C.9})$$

$$g_{*s} \stackrel{(C.2)}{\underset{(C.3)}{\equiv}} 2 + \frac{45}{2\pi^2} \sum_\alpha \frac{\frac{4}{3}\rho_{\nu_\alpha} - \mu_{\nu_\alpha} n_{\nu_\alpha}}{T_\gamma^3 T_{\nu_\alpha}} \quad [\text{thermal distributions}]. \quad (\text{C.10})$$

In eq. (C.10), a factor 2 already appears in the definitions of the thermodynamic functions according to eq. (2.11).

In the late universe, neutrinos become non-relativistic. Then they contribute to the energy density as

$$\Omega_\nu h^2 \equiv \frac{\sum_\alpha m_{\nu_\alpha} (n_{\nu_\alpha} + n_{\bar{\nu}_\alpha})}{\rho_c/h^2} \Big|_{T_\gamma = T_{\text{CMB}}} \stackrel{\text{fast oscillations}}{\simeq} \frac{3}{3} \frac{\sum_\nu m_\nu \sum_\alpha (n_{\nu_\alpha} + n_{\bar{\nu}_\alpha})}{\rho_c/h^2} \Big|_{T_\gamma = T_{\text{CMB}}}, \quad (\text{C.11})$$

where we have assumed that oscillations have equilibrated the number densities. If this assumption is not valid, we should view eq. (C.11) as a definition of what we mean by $\sum_\nu m_\nu$. The critical energy density is defined as $H_0^2 \equiv 8\pi\rho_c/(3m_{\text{pl}}^2)$, and hence $\rho_c/h^2 \equiv 3m_{\text{pl}}^2/(8\pi) \times (100\text{km/s/Mpc})^2 = 8.0959 \times 10^{-11} \text{ eV}^4$. After neutrino decoupling, n_{ν_α} scales as a^{-3} , which in turn scales as T_γ^3 . It is therefore convenient to rewrite eq. (C.11) as

$$\Omega_\nu h^2 \stackrel{T_{\text{CMB}} \leq T_\gamma \leq 0.01 \text{ MeV}}{\simeq} \frac{\sum_\nu m_\nu \sum_\alpha (n_{\nu_\alpha} + n_{\bar{\nu}_\alpha})}{3} \frac{T_{\text{CMB}}^3}{T_\gamma^3} \frac{\rho_c/h^2}{\rho_c/h^2}. \quad (\text{C.12})$$

For the CMB temperature today we take $T_{\text{CMB}} = 2.7255 \text{ K} = 2.34865 \times 10^{-4} \text{ eV}$ [86].

Given a Fortepiano output for eq. (C.7), effective temperatures and chemical potentials are extracted through a matching between the integrated energy and number densities. In particular, at a given photon temperature, parametrized through z (cf. eq. (C.8)), we equate

$$\frac{\rho_\nu}{\rho_\gamma} = \frac{1}{z^4} \frac{1}{2\pi^2/30} \frac{2}{2\pi^2} \int_0^\infty dy y^3 f_\nu(y) \stackrel{(\text{E.9b})}{=} -2 \frac{3T_\nu^4 \text{Li}_4(-e^{\mu_\nu/T_\nu})}{\pi^2} \Big/ \frac{2\pi^2}{30} T_\gamma^4, \quad (\text{C.13})$$

$$\frac{n_\nu}{T_\gamma^3} = \frac{1}{z^3} \frac{2}{2\pi^2} \int_0^\infty dy y^2 f_\nu(y) \stackrel{(\text{E.9a})}{=} -2 \frac{T_\nu^3 \text{Li}_3(-e^{\mu_\nu/T_\nu})}{\pi^2} \Big/ T_\gamma^3. \quad (\text{C.14})$$

The last two cases correspond to a Fermi-Dirac neutrino distribution function, and allow us to extract numerically the dimensionless ratios T_ν/T_γ and μ_ν/T_ν .

3. Comparison of numerical results between Fortepiano and this work

In table I on p. 13, we have highlighted the comparison between our calculations and the results from Fortepiano [69] for integrated quantities. In Fortepiano we have used high-accuracy settings, with the solver precision 10^{-7} and the Gauss-Laguerre method with $N_y = 35$ and $y_{\text{max}} = 20$ for the collision terms. The observables were extracted as described in appendix C2.

From table I we see that describing neutrinos with just their temperature leads to a result for N_{eff} that differs by 0.04% from Fortepiano. This difference is reduced by a factor of two when neutrinos are allowed to have effective chemical potentials. Similar trends are seen in the other quantities. The influence of a neutrino chemical potential is most clear in the energy density parameter of neutrinos today ($\sum m_\nu / [\Omega_\nu h^2 \text{ eV}]$), where the precision increases by a factor of ~ 10 .

Table IV on p. 21 shows a similar comparison, but including more information. In particular, the neutrino temperatures and effective chemical potentials are indicated. The chemical potentials turn out to be quite small, $\sim 5 \times 10^{-3} T_\nu$, but nevertheless they increase the precision significantly. For the Fortepiano's rows, the temperature and chemical potentials are obtained from a matching between the energy density and number density to a Fermi-Dirac distribution, as described by eqs. (C.13) and (C.14). Finally, the last two columns highlight the increase of the neutrino temperature compared to a purely decoupled neutrino, which would have $aT_\nu|_{T_\gamma \ll m_e} / (aT_\nu)|_{T_\gamma \gg m_e} = 1$. This factor enters the relationship between physical and comoving momenta, $q/T_\nu = y/(aT_\nu)$, cf. eq. (C.8).

In fig. 4 we highlight the comparison between our results and those from Fortepiano at the level of the neutrino momentum distribution as a function of y . The four top panels show the comparison for the differential energy density and the four lower ones for the differential number density. Overall, the spectral distortions are small, $< 8 \times 10^{-4}$ in all cases. Including the chemical potentials is important in reducing the spectral distortions both for the number and energy densities, as seen by a comparison of the left ($\mu_\nu = 0$) and right ($\mu_\nu \neq 0$) panels.

All in all, the agreement between the two approaches is excellent both at the level of integrated quantities, such as N_{eff} , h_{eff} or $\Omega_\nu h^2$, but also for the neutrino distribution function, particularly once we include effective chemical potentials.

Neutrino Decoupling in the Standard Model: key parameters and observables extended							
case/parameter	T_γ/T_{ν_e}	T_γ/T_{ν_μ}	T_{ν_e}/μ_{ν_e}	$T_{\nu_\mu}/\mu_{\nu_\mu}$	$(aT_{\nu_e})_{\text{fin}}/(aT_{\nu_e})_{\text{ini}}$	$(aT_{\nu_\mu})_{\text{fin}}/(aT_{\nu_\mu})_{\text{ini}}$	$(aT_\gamma)_{\text{fin}}/(aT_\gamma)_{\text{ini}}$
<i>no oscillations:</i>							
Fortepiano [69]	1.3927	1.3957	-159	-348	-	-	1.3980
this work $\mu_\nu = 0$	1.3946	1.3965	-	-	1.0024	1.0010	1.3979
this work $\mu_\nu \neq 0$	1.3925	1.3956	-152	-341	1.0039	1.0017	1.3979
<i>with oscillations:</i>							
Fortepiano [69]	1.3939	1.3948	-202	-283	-	-	1.3980
this work $\mu_\nu = 0$	1.3958	1.3958	-	-	1.0015	1.0015	1.3978
this work $\mu_\nu \neq 0$	1.3944	1.3944	-234	-234	1.0025	1.0025	1.3979
this work sec. 3	1.3945	1.3944	-297	-215	1.0024	1.0025	1.3979

TABLE IV. Standard Model results as obtained in this work (`nudec_BSM_v2`), by solving for the time evolution of T_γ , T_{ν_e} , T_{ν_μ} , effective neutrino chemical potentials, and the scale factor, a . We compare our results against the Liouville solution from Fortepiano with high accuracy settings [69]. The results include the QED equation of state at $\mathcal{O}(e^3)$, ignoring logarithmic corrections at $\mathcal{O}(e^2)$, and employing the low-energy constants from eq. (A.2). “No oscillations” and “with oscillations” refer to the assumptions in eq. (2.9), or to the more general framework of sec. 3. For the results with Fortepiano, T_ν and μ_ν are not actual temperatures/chemical potentials, but are rather obtained from a fit to the neutrino energy and number densities given by a Fermi-Dirac distribution function, as described by eqs. (C.13) and (C.14).

Appendix D: QED equation of state

The influence of the QED equation-of-state on neutrino decoupling has been extensively discussed in ref. [73]. In this appendix, we comment on ref. [73] in two respects: (i) the contributions of $\mathcal{O}(e^2)$ and $\mathcal{O}(e^3)$ are rewritten with fewer special functions; (ii) the contributions of $\mathcal{O}(e^4)$ and $\mathcal{O}(e^5)$ are worked out in an approximate form, pointing out a new parametric enhancement.

1. General framework and notation

Given that we compare with ref. [73] at several point, we start by summarizing their notation. The evolution equation considered in ref. [73] is eq. (2.1) summed over all species,

$$\dot{\rho}_t + 3H(\rho_t + p_t) \stackrel{(2.1)}{=} 0, \quad (\text{D.1})$$

where the subscript $(\dots)_t$ refers to the total energy density (ρ_t) and pressure (p_t). If we now rescale ρ_t and p_t by powers of the scale factor, a , and replace t through a as the time-like coordinate, eq. (D.1) turns into

$$\frac{d(\rho_t a^4)}{da} = \frac{\rho_t a^4 - 3p_t a^4}{a}. \quad (\text{D.2})$$

Furthermore, we split the energy density and pressure into QED and neutrino parts,

$$\rho_t = \rho + \rho_\nu, \quad \rho_\nu = \sum_\alpha \rho_{\nu_\alpha}, \quad p_t = p + p_\nu, \quad p_\nu = \sum_\alpha p_{\nu_\alpha}, \quad (\text{D.3})$$

where $\rho \equiv \rho_{\text{em}}$ and $p \equiv p_{\text{em}}$ in our notation, and define rescaled variables as

$$x \equiv \frac{a m_e}{(a T_\gamma)_{\text{ini}}}, \quad z \stackrel{(2.8)}{=} \frac{a T_\gamma}{(a T_\gamma)_{\text{ini}}}, \quad \tau \equiv \frac{m_e}{T_\gamma} = \frac{x}{z}, \quad \bar{\rho} \equiv \frac{\rho a^4}{(a T_\gamma)^4}. \quad (\text{D.4})$$

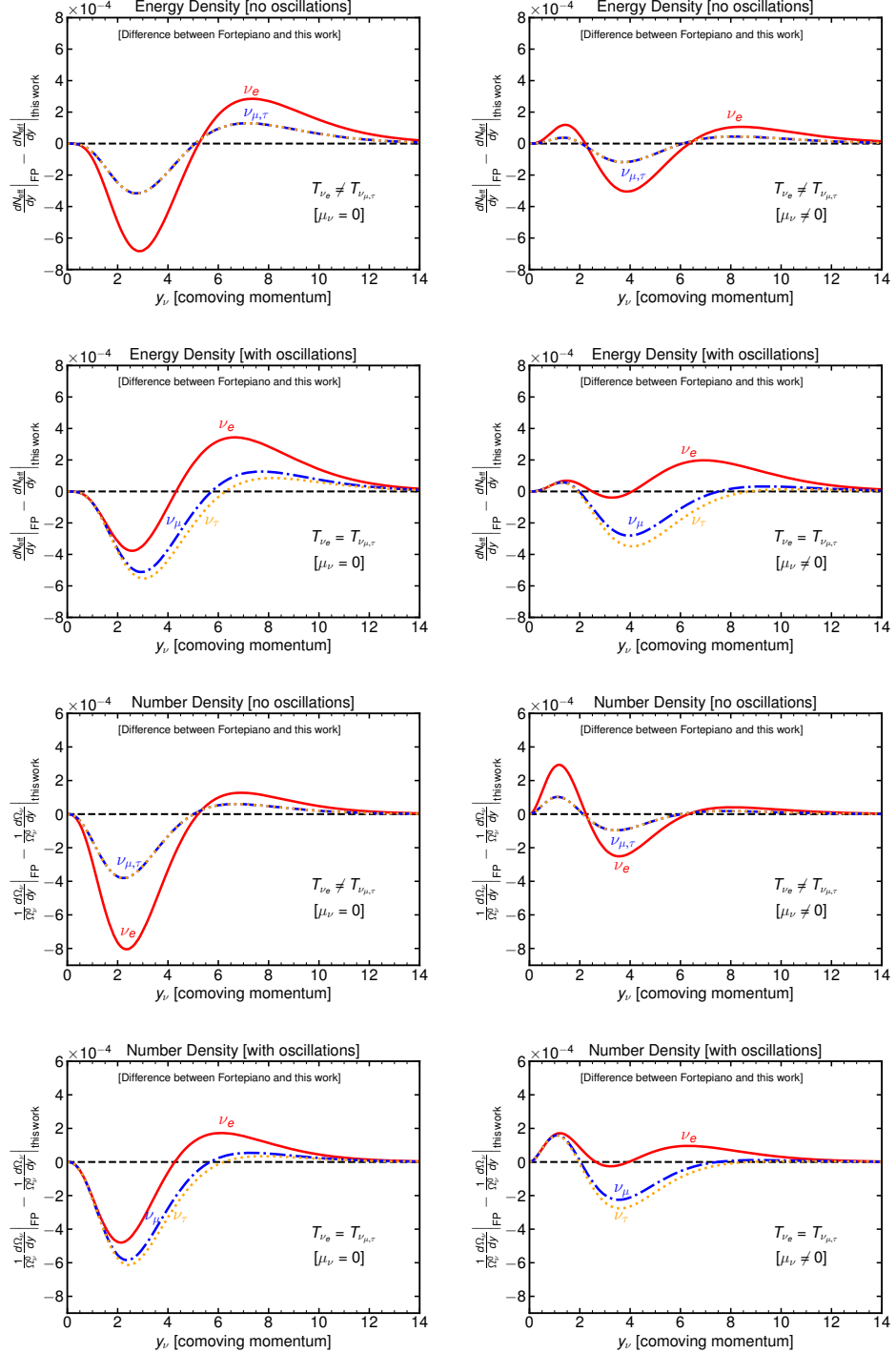


FIG. 4. Comparison of the neutrino distribution function between our results and those obtained in Fortepiano [69]. The four upper panels show the relative difference in terms of the neutrino energy density and the four lower ones for the number density. We can see that the spectral distortions are quite small, $< 8 \times 10^{-4}$. The left panels correspond to solutions with $\mu_\nu = 0$, and the right ones with $\mu_\nu \neq 0$. Including the chemical potentials brings the differences to $< 4 \times 10^{-4}$.

Inserting these rescalings as well as the splitup from eq. (D.3) into eq. (D.2), it turns into

$$\frac{d\bar{\rho}}{dx} = \frac{\bar{\rho} - 3\bar{p}}{x} + \frac{\bar{\rho}_\nu - 3\bar{p}_\nu}{x} - \frac{d\bar{\rho}_\nu}{dx}. \quad (\text{D.5})$$

Subsequently, we write $d/dx = \partial/\partial x + (dz/dx)\partial/\partial z$ on the left-hand side, and then solve for dz/dx , rescaling also the numerator and denominator by the common factor $1/(2z^3)$,

$$\frac{dz}{dx} = \frac{\frac{1}{2z^3} \left[\frac{\bar{\rho} - 3\bar{p}}{x} - \frac{\partial \bar{\rho}}{\partial x} + \frac{\bar{\rho}_\nu - 3\bar{p}_\nu}{x} - \frac{d\bar{\rho}_\nu}{dx} \right]}{\frac{1}{2z^3} \left[\frac{\partial \bar{\rho}}{\partial z} \right]} \underset{\bar{\rho}_\nu - 3\bar{p}_\nu = 0}{\equiv} \frac{\sum_n G_1^{(n)} - \frac{1}{2z^3} \frac{d\bar{\rho}_\nu}{dx}}{\sum_n G_2^{(n)}}. \quad (\text{D.6})$$

Here the QED energy density and pressure have been expanded in a perturbative series, $\bar{\rho} = \sum_n \bar{\rho}^{(n)}$, $\bar{p} = \sum_n \bar{p}^{(n)}$, and we have defined

$$G_1^{(n)} \equiv \frac{1}{2z^3} \left[\frac{\bar{\rho}^{(n)} - 3\bar{p}^{(n)}}{x} - \frac{\partial \bar{\rho}^{(n)}}{\partial x} \right], \quad (\text{D.7})$$

$$G_2^{(n)} \equiv \frac{1}{2z^3} \left[\frac{\partial \bar{\rho}^{(n)}}{\partial z} \right]. \quad (\text{D.8})$$

We note that the factor $1/(2z^3)$ in eq. (D.6) is missing in front of $-d\bar{\rho}_\nu/dx$ in eq. (2.15) of ref. [73].

In order to determine the functions $G_{1,2}^{(n)}$ from eqs. (D.7) and (D.8), the starting point is the pressure (minus the free energy density), from which all other quantities can be derived. Let us write it as

$$p^{(n)} \equiv T_\gamma^4 \tilde{p}^{(n)}(\tau), \quad \tau \stackrel{(\text{D.4})}{=} \frac{m_e}{T_\gamma}. \quad (\text{D.9})$$

Making use of $\partial_{T_\gamma} = -(\tau/T_\gamma)\partial_\tau$, the entropy density ($s = dp/dT_\gamma$), the energy density ($\rho = T_\gamma s - p$), and the “trace anomaly” ($\rho - 3p$) can be obtained as

$$s = T_\gamma^3 (4\tilde{p} - \tau\tilde{p}'), \quad \rho = T_\gamma^4 (3\tilde{p} - \tau\tilde{p}'), \quad \rho - 3p = T_\gamma^4 (-\tau\tilde{p}'). \quad (\text{D.10})$$

The rescaled functions from eqs. (D.4) and (D.5) then take the forms

$$\bar{\rho} \stackrel{(\text{D.10})}{\underset{(\text{D.4})}{=}} z^4 (3\tilde{p} - \tau\tilde{p}'), \quad \bar{\rho} - 3\bar{p} \stackrel{(\text{D.10})}{\underset{(\text{D.4})}{=}} z^4 (-\tau\tilde{p}'). \quad (\text{D.11})$$

Inserting eq. (D.11) into eqs. (D.7) and (D.8), and making use of

$$\partial_x \stackrel{(\text{D.4})}{=} \frac{\partial_\tau}{z}, \quad \partial_z \stackrel{(\text{D.4})}{=} -\frac{\tau\partial_\tau}{z}, \quad (\text{D.12})$$

finally yields

$$G_1 \stackrel{(\text{D.7})}{\underset{(\text{D.11})}{=}} \frac{\tau\tilde{p}'' - 3\tilde{p}'}{2}, \quad G_2 \stackrel{(\text{D.8})}{\underset{(\text{D.11})}{=}} \frac{\tau^2\tilde{p}''}{2} - 3\tau\tilde{p}' + 6\tilde{p}.$$

(D.13)

These relations will be used for determining G_1 and G_2 in the following. We can also give physically more transparent meanings to G_1 and G_2 by taking temperature derivatives directly from the unrescaled pressure, yielding

$$G_1 \stackrel{(\text{D.9})}{\underset{(\text{D.13})}{=}} \frac{1}{2\tau} \left(\frac{\partial_{T_\gamma}^2 p}{T_\gamma^2} - \frac{3\partial_{T_\gamma} p}{T_\gamma^3} \right), \quad G_2 \stackrel{(\text{D.9})}{\underset{(\text{D.13})}{=}} \frac{\partial_{T_\gamma}^2 p}{2T_\gamma^2}. \quad (\text{D.14})$$

We note that the entropy density s , from eq. (D.10), can also be written in terms of G_1 and G_2 . Specifically, adopting

the re-parametrization in terms of h_* from eq. (5.4), and adding the contribution of three kinetically equilibrated neutrinos, we find

$$\boxed{h_* \stackrel{\text{in equilibrium}}{\underset{(5.4)}{\equiv}} \frac{15}{\pi^2} (G_2 - \tau G_1) + \frac{21}{4}}. \quad (\text{D.15})$$

2. Special functions and relations between them

In order to present $G_1(\tau)$ and $G_2(\tau)$, five special functions have been defined in ref. [73],

$$j(\tau) \stackrel{(4.33) \text{ of } [73]}{\equiv} \frac{1}{\pi^2} \int_0^\infty d\omega \frac{\exp(\sqrt{\omega^2 + \tau^2})}{[\exp(\sqrt{\omega^2 + \tau^2}) + 1]^2}, \quad (\text{D.16})$$

$$J(\tau) \stackrel{(2.16) \text{ of } [73]}{\equiv} \frac{1}{\pi^2} \int_0^\infty d\omega \omega^2 \frac{\exp(\sqrt{\omega^2 + \tau^2})}{[\exp(\sqrt{\omega^2 + \tau^2}) + 1]^2}, \quad (\text{D.17})$$

$$Y(\tau) \stackrel{(2.16) \text{ of } [73]}{\equiv} \frac{1}{\pi^2} \int_0^\infty d\omega \omega^4 \frac{\exp(\sqrt{\omega^2 + \tau^2})}{[\exp(\sqrt{\omega^2 + \tau^2}) + 1]^2}, \quad (\text{D.18})$$

$$k(\tau) \stackrel{(4.33) \text{ of } [73]}{\equiv} \frac{1}{\pi^2} \int_0^\infty d\omega \frac{1}{\sqrt{\omega^2 + \tau^2}} \frac{1}{\exp(\sqrt{\omega^2 + \tau^2}) + 1}, \quad (\text{D.19})$$

$$K(\tau) \stackrel{(4.15) \text{ of } [73]}{\equiv} \frac{1}{\pi^2} \int_0^\infty d\omega \frac{\omega^2}{\sqrt{\omega^2 + \tau^2}} \frac{1}{\exp(\sqrt{\omega^2 + \tau^2}) + 1}. \quad (\text{D.20})$$

Furthermore, the derivatives j' , J' , Y' and K' were treated as independent functions, meaning that in total 9 special functions appear in the results of ref. [73]. For completeness and “symmetry”, we here define yet another function,

$$Z(\tau) \equiv \frac{1}{\pi^2} \int_0^\infty d\omega \frac{\omega^4}{\sqrt{\omega^2 + \tau^2}} \frac{1}{\exp(\sqrt{\omega^2 + \tau^2}) + 1}, \quad (\text{D.21})$$

but it is again not independent (see below), and does not appear in the final results.

By making use of partial integrations and algebraic relations, the following identities can be established between the functions defined:

$$J = 2K + \tau^2 k, \quad Y = 4Z + 3\tau^2 K, \quad (\text{D.22})$$

$$Z' = -3\tau K, \quad Y' = -3\tau J, \quad K' = -\tau k, \quad J' = -\tau j, \quad k' = -\frac{j}{\tau}. \quad (\text{D.23})$$

While some of these are easy to verify, by making use of $\omega \partial_\tau f(\sqrt{\omega^2 + \tau^2}) = \tau \partial_\omega f(\sqrt{\omega^2 + \tau^2})$, others may not be obvious. For eq. (D.22), we write $\omega/\sqrt{\omega^2 + \tau^2} = \partial_\omega \sqrt{\omega^2 + \tau^2}$ in the integral representation of K or Z ; carry out a partial integration; and then write $\sqrt{\omega^2 + \tau^2} = (\omega^2 + \tau^2)/\sqrt{\omega^2 + \tau^2}$ in one of the resulting terms. For the last relation in eq. (D.23), we first show that $K' + \tau^2 k' = -\tau(k + j)$, and then subtract the simpler identity $K' = -\tau k$. All in all, eqs. (D.22) and (D.23) permit for a simplification of some of the expressions in ref. [73] (see below).

3. Contribution of $\mathcal{O}(e^0)$

For completeness, let us start at leading order. The pressure, normalized according to eq. (D.9), reads

$$\tilde{p}^{(0)}(\tau) = \frac{\pi^2}{45} + \frac{2Z(\tau)}{3}. \quad (\text{D.24})$$

Inserting into eq. (D.13) and making use of eqs. (D.22) and (D.23), we find

$$G_1^{(0)}(\tau) \stackrel{\substack{(D.24), (D.13) \\ (D.22), (D.23)}}{=} \tau J(\tau), \quad G_2^{(0)}(\tau) \stackrel{\substack{(D.24), (D.13) \\ (D.22), (D.23)}}{=} \tau^2 J(\tau) + Y(\tau) + \frac{2\pi^2}{15}. \quad (\text{D.25})$$

These agree with eq. (2.15) of ref. [73].

4. Contribution of $\mathcal{O}(e^2)$

For the contributions of $\mathcal{O}(e^2)$, we omit all temperature-independent terms from the pressure, and for the moment also one non-factorizable contribution, which is referred to as a ‘‘logarithmic’’ term in ref. [73] (cf. eq. (D.30)). The remainder reads

$$p^{(2)\text{ln}} = -2e^2 \left[\frac{T_\gamma^2}{6} + \int \frac{d^3\mathbf{q}}{(2\pi)^3} \frac{n_F(\epsilon_q)}{\epsilon_q} \right] \int \frac{d^3\mathbf{r}}{(2\pi)^3} \frac{n_F(\epsilon_r)}{\epsilon_r}, \quad (\text{D.26})$$

where $q \equiv |\mathbf{q}|$, $\epsilon_q \equiv \sqrt{q^2 + m_e^2}$, and $n_F(x) \equiv 1/[\exp(x/T_\gamma) + 1]$ is the Fermi distribution. Eq. (D.26) agrees with eq. (4.7) of ref. [73]. Normalized like eq. (D.9), and making use of the special function K from eq. (D.20), it can be expressed as

$$\tilde{p}^{(2)\text{ln}}(\tau) = -\frac{e^2}{2} \left[\frac{1}{3} + K(\tau) \right] K(\tau). \quad (\text{D.27})$$

Inserting into eq. (D.13) and making use of eqs. (D.22) and (D.23), we find

$$G_1^{(2)\text{ln}}(\tau) \stackrel{\substack{(D.27), (D.13) \\ (D.22), (D.23)}}{=} -\frac{e^2\tau}{12} \left\{ j(\tau)[1 + 6K(\tau)] + 2k(\tau)[1 + 3J(\tau)] \right\}, \quad (\text{D.28})$$

$$G_2^{(2)\text{ln}}(\tau) \stackrel{\substack{(D.27), (D.13) \\ (D.22), (D.23)}}{=} -\frac{e^2}{12} \left\{ 3J(\tau) + 2[J(\tau) + K(\tau)][1 + 3J(\tau)] + \tau^2 j(\tau)[1 + 6K(\tau)] \right\}. \quad (\text{D.29})$$

If we employ eqs. (D.22) and (D.23) in the more complicated eqs. (4.13) and (4.14) of ref. [73], or evaluate the results numerically, we find perfect agreement.

For completeness, let us also write down the normally omitted logarithmic term,

$$p^{(2)\text{ln}} = \frac{e^2 m_e^2}{4\pi^4} \int_0^\infty dq \int_0^\infty dr \frac{qr n_F(\epsilon_q) n_F(\epsilon_r)}{\epsilon_q \epsilon_r} \ln \left| \frac{q+r}{q-r} \right|. \quad (\text{D.30})$$

The temperature derivative of this expression agrees with the entropy density given in eq. (4.17) of ref. [73].

We remark that normalizing eq. (D.30) like in eq. (D.9), and differentiating with respect to τ , as needed for computing $G_1^{(2)\text{ln}}$ and $G_2^{(2)\text{ln}}$ from eq. (D.13), leads to complicated expressions. In analogy with eqs. (D.22) and (D.23), there are relations between seemingly different integral representations, which allow to simplify the outcomes. Probably the most compact formulae can be obtained by taking temperature derivatives of eq. (D.30), and extracting then $G_1^{(2)\text{ln}}$ and $G_2^{(2)\text{ln}}$ from eq. (D.14). Introducing the functions

$$\mathcal{A}(\omega_1, \omega_2) \equiv \frac{1}{(e^{\sqrt{\omega_1^2 + \tau^2}} + 1)(e^{\sqrt{\omega_2^2 + \tau^2}} + 1)\sqrt{\omega_1^2 + \tau^2}\sqrt{\omega_2^2 + \tau^2}}, \quad (\text{D.31})$$

$$\mathcal{B}(\omega_1, \omega_2) \equiv \frac{e^{\sqrt{\omega_2^2 + \tau^2}}}{(e^{\sqrt{\omega_1^2 + \tau^2}} + 1)(e^{\sqrt{\omega_2^2 + \tau^2}} + 1)^2\sqrt{\omega_1^2 + \tau^2}}, \quad (\text{D.32})$$

$$\mathcal{C}(\omega_1, \omega_2) \equiv \frac{e^{\sqrt{\omega_2^2 + \tau^2}}}{(e^{\sqrt{\omega_1^2 + \tau^2}} + 1)(e^{\sqrt{\omega_2^2 + \tau^2}} + 1)^2} \left[\frac{e^{\sqrt{\omega_2^2 + \tau^2}}}{e^{\sqrt{\omega_1^2 + \tau^2}} + 1} + \frac{\sqrt{\omega_2^2 + \tau^2}}{\sqrt{\omega_1^2 + \tau^2}} \frac{e^{\sqrt{\omega_2^2 + \tau^2}} - 1}{e^{\sqrt{\omega_1^2 + \tau^2}} + 1} \right], \quad (\text{D.33})$$

we thereby obtain

$$\tilde{p}^{(2)\ln}(\tau) = \frac{e^2\tau^2}{4\pi^4} \int_0^\infty d\omega_1 \int_0^{\omega_1} d\omega_2 \omega_1 \omega_2 \ln \left| \frac{\omega_1 + \omega_2}{\omega_1 - \omega_2} \right| \left[\mathcal{A}(\omega_1, \omega_2) + (\omega_1 \leftrightarrow \omega_2) \right], \quad (\text{D.34})$$

$$G_1^{(2)\ln}(\tau) = \frac{e^2\tau}{4\pi^4} \int_0^\infty d\omega_1 \int_0^{\omega_1} d\omega_2 \omega_1 \omega_2 \ln \left| \frac{\omega_1 + \omega_2}{\omega_1 - \omega_2} \right| \left[\mathcal{C}(\omega_1, \omega_2) - 5\mathcal{B}(\omega_1, \omega_2) + (\omega_1 \leftrightarrow \omega_2) \right], \quad (\text{D.35})$$

$$G_2^{(2)\ln}(\tau) = \frac{e^2\tau^2}{4\pi^4} \int_0^\infty d\omega_1 \int_0^{\omega_1} d\omega_2 \omega_1 \omega_2 \ln \left| \frac{\omega_1 + \omega_2}{\omega_1 - \omega_2} \right| \left[\mathcal{C}(\omega_1, \omega_2) - 2\mathcal{B}(\omega_1, \omega_2) + (\omega_1 \leftrightarrow \omega_2) \right]. \quad (\text{D.36})$$

5. Contribution of $\mathcal{O}(e^3)$

The contribution of $\mathcal{O}(e^3)$ originates from the “Debye mass”,

$$p^{(3)} = \frac{m_{\text{D}}^3 T_\gamma}{12\pi}, \quad m_{\text{D}}^2 = 4e^2 \int \frac{d^3 \mathbf{q}}{(2\pi)^3} \frac{n_{\text{F}}(\epsilon_q)}{\epsilon_q} \left(2 + \frac{m_e^2}{q^2} \right), \quad (\text{D.37})$$

where we use the same notation as in eq. (D.26). Expressed in terms of eq. (D.9), and employing the special functions k and K from eqs. (D.19) and (D.20), respectively, as well as eq. (D.22) to combine them, yields

$$\tilde{p}^{(3)}(\tau) = \frac{e^3}{3\sqrt{2}\pi} [J(\tau)]^{3/2}. \quad (\text{D.38})$$

Inserting into eq. (D.13) and making use of eqs. (D.22) and (D.23), we find

$$G_1^{(3)}(\tau) \stackrel{\substack{(\text{D.38}), (\text{D.13}) \\ (\text{D.22}), (\text{D.23})}}{=} \frac{e^3 \tau}{4\pi} \sqrt{\frac{J(\tau)}{2}} \left[2j(\tau) - \tau j'(\tau) + \frac{\tau^2 j^2(\tau)}{2J(\tau)} \right], \quad (\text{D.39})$$

$$G_2^{(3)}(\tau) \stackrel{\substack{(\text{D.38}), (\text{D.13}) \\ (\text{D.22}), (\text{D.23})}}{=} \frac{e^3}{4\pi} \sqrt{\frac{J(\tau)}{2}} \left[8J(\tau) + 5\tau^2 j(\tau) - \tau^3 j'(\tau) + \frac{\tau^4 j^2(\tau)}{2J(\tau)} \right]. \quad (\text{D.40})$$

Equations (D.39) and (D.40) can be compared with eq. (4.32) of ref. [73]. Our results are simpler; however, making use of eqs. (D.22) and (D.23) in the expressions of ref. [73], or checking numerically, it can be verified that the values are the same.

6. Contributions of $\mathcal{O}(e^4)$ and $\mathcal{O}(e^5)$

We finally discuss the contributions of $\mathcal{O}(e^4)$ and $\mathcal{O}(e^5)$ that were *not* included in ref. [73]. These terms have been fully determined only in the massless limit ($\tau = m_e/T_\gamma \rightarrow 0$), and we start by recalling those results. However, we can subsequently upgrade parts of the expressions to the massive situation, by making use of renormalization group invariance, as discussed around eqs. (4.1)–(4.3).

The finite coefficients c_4 and c_5 were first determined in ref. [87], however c_4 was computed only numerically, and the renormalization scale was fixed in a non-standard way. An analytic computation of c_4 can be found in ref. [88],

$$\begin{aligned} c_4 &\stackrel{(5.1) \text{ of [88]}}{=} -\frac{5}{(4\pi)^4} \left[\frac{20}{3} \ln(4\pi) + \frac{8}{3} \frac{\zeta'(-3)}{\zeta(-3)} - \frac{16}{3} \frac{\zeta'(-1)}{\zeta(-1)} - 4\gamma_E - \frac{319}{12} + \frac{208 \ln 2}{5} \right] \\ &\stackrel{(5.3) \text{ of [88]}}{\approx} -0.00159412. \end{aligned} \quad (\text{D.41})$$

An independent computation of c_5 , with a general renormalization scale so that the non-logarithmic part can be easily isolated, can be found in ref. [89],

$$c_5 \stackrel{(4.3) \text{ of [89]}}{=} \frac{320}{\sqrt{3}(4\pi)^5} \left[\ln(4\pi) - \gamma_E - \frac{7}{4} - 2\ln 2 \right] \approx -0.000697166. \quad (\text{D.42})$$

The coefficients c_4 and c_5 will be needed in eqs. (D.46) and (D.48), respectively.

We now move on to the massive case. The pressure can still be written like in eq. (4.1), however the coefficients c_n become functions of $\tau = m_e/T_\gamma$. We fix the renormalization scale as $\bar{\mu} = m_e$, whereby the logarithms turn into $\ln \tau$. Fixing the values of \tilde{c}_4 and \tilde{c}_5 according to eq. (4.3), and going over to the normalization in eq. (D.9), we then find

$$\tilde{p}^{(4)}(\tau) \underset{(4.3)}{\approx}^{\text{(D.43),(D.9)}} -\frac{e^2 \tilde{p}^{(2)} \ln(\tau) \ln \tau}{6\pi^2} + \frac{c_4 e^4 \pi^2}{45}, \quad (\text{D.43})$$

$$\tilde{p}^{(5)}(\tau) \underset{(4.3)}{\approx}^{\text{(D.43),(D.9)}} -\frac{e^2 \tilde{p}^{(3)}(\tau) \ln \tau}{4\pi^2} + \frac{c_5 e^5 \pi^2}{45}, \quad (\text{D.44})$$

where $\tilde{p}^{(2)}$ and $\tilde{p}^{(3)}$ are given by eqs. (D.27) and (D.38), respectively. While the logarithmic terms are fixed by renormalization group invariance, the τ -dependence of c_4 and c_5 is unknown, so we treat them as constants, as is appropriate for the massless limit.

Subsequently, we can insert eqs. (D.43) and (D.44) into eq. (D.13), in order to estimate the functions $G_{1,2}^{(4,5)}$. At $\mathcal{O}(e^4)$ we find

$$G_1^{(4)}(\tau) \underset{\text{(D.13)}}{\approx}^{\text{(D.43)}} -\frac{e^2 G_1^{(2)} \ln(\tau) \ln \tau}{6\pi^2} - \frac{e^4}{36\pi^2} \frac{J(\tau) + 6[J(\tau) - K(\tau)]K(\tau)}{\tau}, \quad (\text{D.45})$$

$$G_2^{(4)}(\tau) \underset{\text{(D.13)}}{\approx}^{\text{(D.43)}} -\frac{e^2 G_2^{(2)} \ln(\tau) \ln \tau}{6\pi^2} + \frac{2c_4 e^4 \pi^2}{15} - \frac{e^4}{72\pi^2} \left\{ 3K(\tau)[1 - K(\tau)] + 2J(\tau)[1 + 6K(\tau)] \right\}, \quad (\text{D.46})$$

where $G_1^{(2)\ln}$ and $G_2^{(2)\ln}$ are given by eqs. (D.28) and (D.29), respectively. An analogous computation at $\mathcal{O}(e^5)$ produces

$$G_1^{(5)}(\tau) \underset{\text{(D.13)}}{\approx}^{\text{(D.44)}} -\frac{e^2 G_1^{(3)}(\tau) \ln \tau}{4\pi^2} + \frac{e^5}{24\pi^3} \sqrt{\frac{J(\tau)}{2}} \frac{4J(\tau) + 3\tau^2 j(\tau)}{\tau}, \quad (\text{D.47})$$

$$G_2^{(5)}(\tau) \underset{\text{(D.13)}}{\approx}^{\text{(D.44)}} -\frac{e^2 G_2^{(3)}(\tau) \ln \tau}{4\pi^2} + \frac{2c_5 e^5 \pi^2}{15} + \frac{e^5}{24\pi^3} \sqrt{\frac{J(\tau)}{2}} \left\{ 7J(\tau) + 3\tau^2 j(\tau) \right\}, \quad (\text{D.48})$$

where $G_1^{(3)}$ and $G_2^{(3)}$ are given by eqs. (D.39) and (D.40), respectively.

We note from eqs. (D.45) and (D.47) that G_1 obtains a $1/\tau$ -enhancement at $\tau = m_e/T_\gamma \ll 1$ at $\mathcal{O}(e^4)$ and $\mathcal{O}(e^5)$. This is not a coincidence. It can be seen from eq. (4.1) that in the limit $\tau \rightarrow 0$, when the c_n 's are constants, \tilde{c}_4 and \tilde{c}_5 are the first coefficients contributing to \tilde{p}' , and therefore to the trace anomaly, cf. eq. (D.10). However, despite the small- τ enhancement of $G_1^{(4)}$ and $G_1^{(5)}$, in the end we find *no* substantial numerical effect on N_{eff} or h_{eff} from them.

Appendix E: Bessel and polylogarithmic representations of thermodynamic quantities

One novelty of our numerical packages is the option to evaluate thermodynamic formulae as a series in modified Bessel functions. In this appendix we document the relevant formulae and mention their possible limitations.

1. Neutrino and BSM sectors

Considering non-interacting bosons (–) or fermions (+) with g internal degrees of freedom, their number density, energy density and pressure are written as (cf. eq. (2.11))

$$n_\pm \stackrel{\text{(2.11)}}{=} \frac{g}{2\pi^2} \int_m^\infty dE E \sqrt{E^2 - m^2} f_\pm, \quad (\text{E.1a})$$

$$\rho_{\pm} \stackrel{(E.11)}{=} \frac{g}{2\pi^2} \int_m^{\infty} dE E^2 \sqrt{E^2 - m^2} f_{\pm}, \quad (E.1b)$$

$$p_{\pm} \stackrel{(E.11)}{=} \frac{g}{6\pi^2} \int_m^{\infty} dE (E^2 - m^2)^{3/2} f_{\pm}. \quad (E.1c)$$

We include bosons, as they appear in BSM constructions. The distribution functions have the Bose or Fermi shape,

$$f_{\pm} = \frac{1}{e^{(E-\mu)/T} \pm 1} \begin{array}{l} + [\text{fermions}] \\ - [\text{bosons}] \end{array}. \quad (E.2)$$

For $m > 0$ the integrals in eqs. (E.1a)–(E.1c) are not analytically solvable, however they can be written as a sum of Bessel functions [90]. If $\mu < m$, so that $\mu < E$, we can write down a convergent geometric series,⁷

$$f_{\pm} = \frac{e^{(\mu-E)/T}}{1 \pm e^{(\mu-E)/T}} \stackrel{\mu \leq E}{=} \sum_{n=0}^{\infty} (\mp 1)^n [e^{\mu/T}]^{n+1} [e^{-E/T}]^{n+1}. \quad (E.4)$$

In usual scenarios without particle-antiparticle asymmetries, chemical potentials tend to be negative, so we can employ eq. (E.4). For massless fermions, results applying to both signs can be derived from eq. (E.3), and are given in eqs. (E.9a)–(E.9c).

Recalling now representations of the generalized Bessel function K_{ν} ,

$$K_{\nu}(z) \stackrel{\substack{\text{Re } z > 0 \\ \text{Re } \nu > -\frac{1}{2}}}{=} \frac{\sqrt{\pi} \left(\frac{z}{2}\right)^{\nu}}{\Gamma(\nu + \frac{1}{2})} \int_1^{\infty} dt e^{-zt} (t^2 - 1)^{\nu - \frac{1}{2}}, \quad (E.5a)$$

$$K_{\nu+1}(z) \stackrel{\substack{\text{Re } z > 0 \\ \text{Re } \nu > -\frac{1}{2}}}{=} \frac{\sqrt{\pi} \left(\frac{z}{2}\right)^{\nu}}{\Gamma(\nu + \frac{1}{2})} \int_1^{\infty} dt t e^{-zt} (t^2 - 1)^{\nu - \frac{1}{2}}, \quad (E.5b)$$

we can rewrite all the thermodynamic integrals in terms of sums of Bessel functions,

$$n_{\pm} \stackrel{\substack{(E.1a) \\ (E.4), (E.5)}}{=} \frac{g}{2\pi^2} \sum_{n=0}^{\infty} \frac{m^2 T}{n+1} (\mp 1)^n e^{\frac{\mu(n+1)}{T}} K_2 \left[\frac{m(n+1)}{T} \right], \quad (E.6a)$$

$$\rho_{\pm} \stackrel{\substack{(E.1b) \\ (E.4), (E.5)}}{=} \frac{g}{2\pi^2} \sum_{n=0}^{\infty} \frac{m^2 T}{(n+1)^2} (\mp 1)^n e^{\frac{\mu(n+1)}{T}} \left\{ m(n+1) K_1 \left[\frac{m(n+1)}{T} \right] + 3T K_2 \left[\frac{m(n+1)}{T} \right] \right\}, \quad (E.6b)$$

$$p_{\pm} \stackrel{\substack{(E.1c) \\ (E.4), (E.5)}}{=} \frac{g}{2\pi^2} \sum_{n=0}^{\infty} \frac{m^2 T^2}{(n+1)^2} (\mp 1)^n e^{\frac{\mu(n+1)}{T}} K_2 \left[\frac{m(n+1)}{T} \right]. \quad (E.6c)$$

For eqs. (2.3a) and (2.3b) we also need derivatives with respect to T and μ , which can be obtained with the recursion relations $-z K'_{\nu} = \nu K_{\nu} + z K_{\nu-1}$ and $K_{\nu+1} = K_{\nu-1} + (2\nu/z) K_{\nu}$, as

$$\frac{\partial n_{\pm}}{\partial T} = \frac{g}{2\pi^2} \sum_{n=0}^{\infty} \frac{m^2}{T} (\mp 1)^n e^{\frac{\mu(n+1)}{T}} \left\{ m K_1 \left[\frac{m(n+1)}{T} \right] + \left(\frac{3T}{n+1} - \mu \right) K_2 \left[\frac{m(n+1)}{T} \right] \right\}, \quad (E.7a)$$

$$\begin{aligned} \frac{\partial \rho_{\pm}}{\partial T} = & \frac{g}{2\pi^2} \sum_{n=0}^{\infty} \frac{m}{(n+1)^2 T} (\mp 1)^n e^{\frac{\mu(n+1)}{T}} \left\{ m [m^2(n+1)^2 + 3T(4T - \mu(n+1))] K_0 \left[\frac{m(n+1)}{T} \right] \right. \\ & \left. + \frac{1}{n+1} [m^2(n+1)^2(5T - \mu(n+1)) + 6T^2(4T - \mu(n+1))] K_1 \left[\frac{m(n+1)}{T} \right] \right\}, \end{aligned} \quad (E.7b)$$

⁷ If $\mu > m$, there is an energy domain in which we need to expand in $e^{(E-\mu)/T}$ instead, leading to the generalized representation

$$f_{\pm} = \theta(E - \mu) \sum_{n=0}^{\infty} (\mp 1)^n [e^{\mu/T}]^{n+1} [e^{-E/T}]^{n+1} - \theta(\mu - E) \sum_{n=0}^{\infty} (\mp 1)^{n+1} [e^{-\mu/T}]^n [e^{E/T}]^n. \quad (E.3)$$

$$\frac{\partial n_{\pm}}{\partial \mu} = \frac{g}{2\pi^2} \sum_{n=0}^{\infty} m^2 (\mp 1)^n e^{\frac{\mu(n+1)}{T}} K_2 \left[\frac{m(n+1)}{T} \right], \quad (\text{E.7c})$$

$$\frac{\partial \rho_{\pm}}{\partial \mu} = \frac{g}{2\pi^2} \sum_{n=0}^{\infty} \frac{m^2}{n+1} (\mp 1)^n e^{\frac{\mu(n+1)}{T}} \left\{ m(n+1) K_1 \left[\frac{m(n+1)}{T} \right] + 3T K_2 \left[\frac{m(n+1)}{T} \right] \right\}. \quad (\text{E.7d})$$

The Maxwell-Boltzmann limit is given by the $n = 0$ term. In practice, we set $n_{\max} = 30$ by default in the code.

In the massless limit, applicable to neutrinos, the results can be given in terms of polylogarithms. For $|z| < 1$, a polylogarithm is defined through

$$\text{Li}_s(z) \stackrel{|z| \leq 1}{=} \sum_{n=1}^{\infty} \frac{z^n}{n^s}, \quad (\text{E.8})$$

but it can be analytically continued outside of this domain. To obtain convergent sum representations, we use eq. (E.3) as a starting point, leading to

$$\begin{aligned} n_+ &\stackrel{\substack{(\text{E.1a}) \\ (\text{E.3}), (\text{E.8})}}{=} \frac{g}{\pi^2} \left[-T^3 \text{Li}_3 \left(-e^{-\frac{|\mu|}{T}} \right) + \theta(\mu) \frac{\mu(\mu^2 + \pi^2 T^2)}{6} \right] \\ &\stackrel{\substack{\text{analytic} \\ \text{continuation}}}{=} \frac{g}{\pi^2} \left[-T^3 \text{Li}_3 \left(-e^{\frac{\mu}{T}} \right) \right], \end{aligned} \quad (\text{E.9a})$$

$$\begin{aligned} \rho_+ &\stackrel{\substack{(\text{E.1b}) \\ (\text{E.3}), (\text{E.8})}}{=} \frac{g}{\pi^2} \left[3T^4 \text{sign}(\mu) \text{Li}_4 \left(-e^{-\frac{|\mu|}{T}} \right) + \theta(\mu) \left(\frac{\mu^4}{8} + \frac{(\mu\pi T)^2}{4} + \frac{7(\pi T)^4}{120} \right) \right] \\ &\stackrel{\substack{\text{analytic} \\ \text{continuation}}}{=} \frac{g}{\pi^2} \left[-3T^4 \text{Li}_4 \left(-e^{\frac{\mu}{T}} \right) \right], \end{aligned} \quad (\text{E.9b})$$

$$p_+ \stackrel{\substack{(\text{E.1b}) \\ (\text{E.1c})}}{=} \frac{\rho_+}{3}. \quad (\text{E.9c})$$

Making use of $\partial_z \text{Li}_s(-e^z) = \text{Li}_{s-1}(-e^z)$, one can easily find partial temperature and chemical potential derivatives. Moreover, for massless bosons, we note from eq. (E.2) that $f_+|_{\mu \rightarrow \mu + i\pi T} = -f_-$, though then a branch cut opens at $\mu = 0$, and the representations are only valid for $\mu < 0$. The resulting expressions are given in table V on p. 30.

2. Accuracy & code speed-up

We have checked the accuracy of the series representations in eqs. (E.6a)–(E.6c), after restricting to $n_{\max} = 30$. Even though the series correspond to low-temperature expansions, their convergent nature guarantees that they can also be applied for $T > m$. Restricting to $T < 100m$, the given n_{\max} yields the error ($-$ = bosons, $+$ = fermions)

$$\delta n_- < 5 \times 10^{-4}, \quad \delta n_+ < 10^{-5}, \quad \delta \rho_- < 10^{-5}, \quad \delta \rho_+ < 10^{-6}, \quad \delta p_- < 10^{-5}, \quad \delta p_+ < 10^{-6}. \quad (\text{E.10})$$

Inserting $\mu < 0$ accelerates the convergence. On the other hand, for $\mu > m > 0$, the series are not convergent, but for fermions they still work reasonably well, provided that the chemical potentials are not too large. For massless fermions, we can use eqs. (E.9a)–(E.9c) for either sign.

The speed-up of the code from using series expansions rather than integrating the functions numerically each time they are called, is a factor of 12 in **Mathematica**, and similarly in **python**. We have seen this both in the Standard Model, but also in the case of a $\phi \leftrightarrow \nu\bar{\nu}$ BSM scenario.

massless thermodynamics, $m = 0$, $x \equiv e^{\mu/T}$			
quantity	Fermi-Dirac	Bose-Einstein ($\mu < 0$)	Maxwell-Boltzmann
n	$-g \frac{T^3}{\pi^2} \text{Li}_3(-x)$	$g \frac{T^3}{\pi^2} \text{Li}_3(x)$	$g \frac{T^3}{\pi^2} x$
ρ	$-g \frac{3T^4}{\pi^2} \text{Li}_4(-x)$	$g \frac{3T^4}{\pi^2} \text{Li}_4(x)$	$g \frac{3T^4}{\pi^2} x$
p	$\rho/3$	$\rho/3$	$\rho/3$
$\partial n/\partial T$	$g \frac{T(\mu \text{Li}_2(-x) - 3T \text{Li}_3(-x))}{\pi^2}$	$g \frac{T(3T \text{Li}_3(x) - \mu \text{Li}_2(x))}{\pi^2}$	$g \frac{T(3T - \mu)}{\pi^2} x$
$\partial \rho/\partial T$	$g \frac{3T^2(\mu \text{Li}_3(-x) - 4T \text{Li}_4(-x))}{\pi^2}$	$g \frac{3T^2(4T \text{Li}_4(x) - \mu \text{Li}_3(x))}{\pi^2}$	$g \frac{3T^2(4T - \mu)}{\pi^2} x$
$\partial n/\partial \mu$	$-g \frac{T^2}{\pi^2} \text{Li}_2(-x)$	$g \frac{T^2}{\pi^2} \text{Li}_2(x)$	$g \frac{T^2}{\pi^2} x$
$\partial \rho/\partial \mu$	$-g \frac{3T^3}{\pi^2} \text{Li}_3(-x)$	$g \frac{3T^3}{\pi^2} \text{Li}_3(x)$	$g \frac{3T^3}{\pi^2} x$

massless thermodynamics, $m = 0$, $\mu = 0$			
quantity	Fermi-Dirac	Bose-Einstein	Maxwell-Boltzmann
n	$g \frac{3}{4} \frac{\zeta(3)}{\pi^2} T^3$	$g \frac{\zeta(3)}{\pi^2} T^3$	$g \frac{T^3}{\pi^2}$
ρ	$g \frac{7}{8} \frac{\pi^2}{30} T^4$	$g \frac{\pi^2}{30} T^4$	$g \frac{3T^4}{\pi^2}$
p	$\rho/3$	$\rho/3$	$\rho/3$
$\partial n/\partial T$	$3n/T$	$3n/T$	$3n/T$
$\partial \rho/\partial T$	$4\rho/T$	$4\rho/T$	$4\rho/T$

TABLE V. Summary of results contained in, or derivable from eqs. (E.9a)–(E.9c). The bosonic expressions originate from the analytic continuation $f_+|_{\mu \rightarrow \mu + i\pi T} = -f_-$, but are only valid for $\mu < 0$. The Maxwell-Boltzmann limits were obtained from eqs. (E.6a)–(E.7d), by restricting to $n = 0$ and employing $K_\nu(z) \approx 2^{\nu-1}\Gamma(\nu)z^{-\nu}$ for $|z| \ll 1$. In the lower panel, $\zeta(3) = \text{Li}_3(1) = -(4/3)\text{Li}_3(-1) \approx 1.20206$ and $\pi^4/90 = \text{Li}_4(1) = -(8/7)\text{Li}_4(-1)$.

3. QED sector

As described in appendix D, six functions are needed in order to describe QED corrections to the electromagnetic energy density and pressure of the universe (provided that we neglect the logarithmic term of $\mathcal{O}(e^2)$). They can be written as sums over Bessel functions similarly to eqs. (E.6a)–(E.7d), making use eq. (E.4) as well as the related expansion

$$\frac{e^x}{(e^x + 1)^2} = \sum_{n=0}^{\infty} (-1)^n (n+1) e^{-x(n+1)}. \quad (\text{E.11})$$

Inserting also the recursion relation $K_1(z) + zK'_1(z) = -zK_0(z)$, we find

$$j(\tau) \stackrel{(\text{D.16})}{=} \frac{1}{\pi^2} \sum_{n=0}^{\infty} (-1)^n (n+1) \tau K_1[(n+1)\tau], \quad (\text{E.12})$$

$$j'(\tau) \stackrel{(E.12)}{=} \frac{1}{\pi^2} \sum_{n=0}^{\infty} (-1)^{n+1} (n+1)^2 \tau K_0[(n+1)\tau], \quad (E.13)$$

$$J(\tau) \stackrel{(D.17)}{=} \frac{1}{\pi^2} \sum_{n=0}^{\infty} (-1)^n \tau^2 K_2[(n+1)\tau], \quad (E.14)$$

$$Y(\tau) \stackrel{(D.18)}{=} \frac{1}{\pi^2} \sum_{n=0}^{\infty} \frac{3(-1)^n \tau^3 K_3[(n+1)\tau]}{n+1}, \quad (E.15)$$

$$k(\tau) \stackrel{(D.19)}{=} \frac{1}{\pi^2} \sum_{n=0}^{\infty} (-1)^n K_0[(n+1)\tau], \quad (E.16)$$

$$K(\tau) \stackrel{(D.20)}{=} \frac{1}{\pi^2} \sum_{n=0}^{\infty} \frac{(-1)^n \tau K_1[(n+1)\tau]}{n+1}, \quad (E.17)$$

$$Z(\tau) \stackrel{(D.21)}{=} \frac{1}{\pi^2} \sum_{n=0}^{\infty} \frac{3(-1)^n \tau^2 K_2[(n+1)\tau]}{(n+1)^2}. \quad (E.18)$$

For most of these we can use $n_{\max} = 30$ if we restrict to $\tau > 0.01$ (i.e. $T_\gamma < 100m_e$), and then the speed-up is a factor of ~ 10 compared with an exact integration. However, the functions $j(\tau)$ and $k(\tau)$ require $n_{\max} = 1000$ for a comparable precision, and $j'(\tau)$ requires $n_{\max} = 3000$. As τ increases, convergence accelerates, though only for $\tau > 0.5$ is $n_{\max} = 30$ sufficient for $j'(\tau)$. Otherwise, we can use small- τ expansions instead, in particular $j(\tau) \approx [1 + 7\zeta'(-2)\tau^2]/(2\pi^2)$, $j'(\tau) \approx 7\zeta'(-2)\tau/\pi^2$, $J(\tau) \approx [2\pi^2 - 3\tau^2]/(12\pi^2)$, $Y(\tau) \approx [14\pi^2 - 15\tau^2]/60$, $k(\tau) \approx [\ln(\pi/\tau) - \gamma_E]/(2\pi^2)$, $K(\tau) \approx [\pi^2 + 3\tau^2 \ln(\tau)]/(12\pi^2)$, $Z(\tau) \approx [7\pi^2 - 15\tau^2]/120$.

- [1] E. Komatsu *et al.* (WMAP), Five-Year Wilkinson Microwave Anisotropy Probe (WMAP) Observations: Cosmological Interpretation, *Astrophys. J. Suppl.* **180**, 330 (2009), arXiv:0803.0547 [astro-ph].
- [2] P. A. R. Ade *et al.* (Planck), Planck 2013 results. XVI. Cosmological parameters, *Astron. Astrophys.* **571**, A16 (2014), arXiv:1303.5076 [astro-ph.CO].
- [3] N. Aghanim *et al.* (Planck), Planck 2018 results. VI. Cosmological parameters, *Astron. Astrophys.* **641**, A6 (2020), [Erratum: *Astron. Astrophys.* 652, C4 (2021)], arXiv:1807.06209 [astro-ph.CO].
- [4] T. Louis *et al.* (ACT), The Atacama Cosmology Telescope: DR6 Power Spectra, Likelihoods and Λ CDM Parameters, (2025), arXiv:2503.14452 [astro-ph.CO].
- [5] E. Calabrese *et al.* (ACT), The Atacama Cosmology Telescope: DR6 Constraints on Extended Cosmological Models, (2025), arXiv:2503.14454 [astro-ph.CO].
- [6] E. Camphuis *et al.* (SPT-3G), SPT-3G D1: CMB temperature and polarization power spectra and cosmology from 2019 and 2020 observations of the SPT-3G Main field, (2025), arXiv:2506.20707 [astro-ph.CO].
- [7] K. Prabhu *et al.* (SPT-3G), Testing the Λ CDM Cosmological Model with Forthcoming Measurements of the Cosmic Microwave Background with SPT-3G, *Astrophys. J.* **973**, 4 (2024), arXiv:2403.17925 [astro-ph.CO].
- [8] P. Ade *et al.* (Simons Observatory), The Simons Observatory: Science goals and forecasts, *JCAP* **02**, 056 (2019), arXiv:1808.07445 [astro-ph.CO].
- [9] Y. I. Izotov, T. X. Thuan, and N. G. Guseva, A new determination of the primordial He abundance using the He I $\lambda 10830\text{\AA}$ emission line: cosmological implications, *Mon. Not. Roy. Astron. Soc.* **445**, 778 (2014), arXiv:1408.6953 [astro-ph.CO].
- [10] E. Aver, D. A. Berg, K. A. Olive, R. W. Pogge, J. J. Salzer, and E. D. Skillman, Improving helium abundance determinations with Leo P as a case study, *JCAP* **03**, 027 (2021), arXiv:2010.04180 [astro-ph.CO].
- [11] R. J. Cooke, M. Pettini, and C. C. Steidel, One Percent Determination of the Primordial Deuterium Abundance, *Astrophys. J.* **855**, 102 (2018), arXiv:1710.11129 [astro-ph.CO].
- [12] V. Mossa *et al.*, The baryon density of the Universe from an improved rate of deuterium burning, *Nature* **587**, 210 (2020).
- [13] O. Pisanti, G. Mangano, G. Miele, and P. Mazzella, Primordial Deuterium after LUNA: concordances and error budget, *JCAP* **04**, 020 (2021), arXiv:2011.11537 [astro-ph.CO].
- [14] C. Pitrou, A. Coc, J.-P. Uzan, and E. Vangioni, A new tension in the cosmological model from primordial deuterium?, *Mon. Not. Roy. Astron. Soc.* **502**, 2474 (2021), arXiv:2011.11320 [astro-ph.CO].

- [15] T.-H. Yeh, J. Shelton, K. A. Olive, and B. D. Fields, Probing physics beyond the standard model: limits from BBN and the CMB independently and combined, *JCAP* **10**, 046 (2022), arXiv:2207.13133 [astro-ph.CO].
- [16] C. Boehm and P. Fayet, Scalar dark matter candidates, *Nucl. Phys. B* **683**, 219 (2004), arXiv:hep-ph/0305261.
- [17] J. L. Feng and J. Kumar, The WIMPless Miracle: Dark-Matter Particles without Weak-Scale Masses or Weak Interactions, *Phys. Rev. Lett.* **101**, 231301 (2008), arXiv:0803.4196 [hep-ph].
- [18] C. Boehm, M. J. Dolan, and C. McCabe, A Lower Bound on the Mass of Cold Thermal Dark Matter from Planck, *JCAP* **08**, 041 (2013), arXiv:1303.6270 [hep-ph].
- [19] S. Knapen, T. Lin, and K. M. Zurek, Light Dark Matter: Models and Constraints, *Phys. Rev. D* **96**, 115021 (2017), arXiv:1709.07882 [hep-ph].
- [20] N. Sabti, J. Alvey, M. Escudero, M. Fairbairn, and D. Blas, Refined Bounds on MeV-scale Thermal Dark Sectors from BBN and the CMB, *JCAP* **01**, 004 (2020), arXiv:1910.01649 [hep-ph].
- [21] M. Pospelov, A. Ritz, and M. B. Voloshin, Secluded WIMP Dark Matter, *Phys. Lett. B* **662**, 53 (2008), arXiv:0711.4866 [hep-ph].
- [22] P. Ilten, Y. Soreq, M. Williams, and W. Xue, Serendipity in dark photon searches, *JHEP* **06**, 004 (2018), arXiv:1801.04847 [hep-ph].
- [23] M. Bauer, P. Foldenauer, and J. Jaeckel, Hunting All the Hidden Photons, *JHEP* **07**, 094 (2018), arXiv:1803.05466 [hep-ph].
- [24] M. Escudero, D. Hooper, G. Krnjaic, and M. Pierre, Cosmology with A Very Light $L_\mu - L_\tau$ Gauge Boson, *JHEP* **03**, 071 (2019), arXiv:1901.02010 [hep-ph].
- [25] H. Esseili and G. D. Kribs, Cosmological implications of gauged $U(1)_{B-L}$ on ΔN_{eff} in the CMB and BBN, *JCAP* **05**, 110 (2024), arXiv:2308.07955 [hep-ph].
- [26] F. Bezrukov and D. Gorbunov, Light inflaton Hunter's Guide, *JHEP* **05**, 010 (2010), arXiv:0912.0390 [hep-ph].
- [27] G. Krnjaic, Probing Light Thermal Dark-Matter With a Higgs Portal Mediator, *Phys. Rev. D* **94**, 073009 (2016), arXiv:1512.04119 [hep-ph].
- [28] M. W. Winkler, Decay and detection of a light scalar boson mixing with the Higgs boson, *Phys. Rev. D* **99**, 015018 (2019), arXiv:1809.01876 [hep-ph].
- [29] A. Fradette, M. Pospelov, J. Pradler, and A. Ritz, Cosmological beam dump: constraints on dark scalars mixed with the Higgs boson, *Phys. Rev. D* **99**, 075004 (2019), arXiv:1812.07585 [hep-ph].
- [30] D. Cadamuro and J. Redondo, Cosmological bounds on pseudo Nambu-Goldstone bosons, *JCAP* **02**, 032 (2012), arXiv:1110.2895 [hep-ph].
- [31] P. F. Depta, M. Hufnagel, and K. Schmidt-Hoberg, Robust cosmological constraints on axion-like particles, *JCAP* **05**, 009 (2020), arXiv:2002.08370 [hep-ph].
- [32] M. Jain, A. Maggi, W.-Y. Ai, and D. J. E. Marsh, New insights into axion freeze-in, *JHEP* **11**, 166 (2024), [Erratum: *JHEP* 04, 156 (2025)], arXiv:2406.01678 [hep-ph].
- [33] K. Bouzoud and J. Ghiglieri, Thermal axion production at hard and soft momenta, *JHEP* **01**, 163 (2025), arXiv:2404.06113 [hep-ph].
- [34] M. Escudero, C. Garcia-Perez, and M. Ovchynnikov, Nucleosynthesis and CMB bounds on photophilic ALPs: a fresh look, (2025), arXiv:2511.00157 [hep-ph].
- [35] A. D. Dolgov, S. H. Hansen, G. Raffelt, and D. V. Semikoz, Heavy sterile neutrinos: Bounds from big bang nucleosynthesis and SN1987A, *Nucl. Phys. B* **590**, 562 (2000), arXiv:hep-ph/0008138.
- [36] P. Hernández, M. Kekic, and J. Lopez-Pavon, N_{eff} in low-scale seesaw models versus the lightest neutrino mass, *Phys. Rev. D* **90**, 065033 (2014), arXiv:1406.2961 [hep-ph].
- [37] A. Boyarsky, M. Ovchynnikov, O. Ruchayskiy, and V. Syvolap, Improved big bang nucleosynthesis constraints on heavy neutral leptons, *Phys. Rev. D* **104**, 023517 (2021), arXiv:2008.00749 [hep-ph].
- [38] J. Alexander *et al.*, Dark Sectors 2016 Workshop: Community Report (2016) arXiv:1608.08632 [hep-ph].
- [39] J. Beacham *et al.*, Physics Beyond Colliders at CERN: Beyond the Standard Model Working Group Report, *J. Phys. G* **47**, 010501 (2020), arXiv:1901.09966 [hep-ex].
- [40] C. Antel *et al.*, Feebly-interacting particles: FIPs 2022 Workshop Report, *Eur. Phys. J. C* **83**, 1122 (2023), arXiv:2305.01715 [hep-ph].
- [41] S. Hannestad and J. Madsen, Neutrino decoupling in the early universe, *Phys. Rev. D* **52**, 1764 (1995), arXiv:astro-ph/9506015.
- [42] A. D. Dolgov, S. H. Hansen, and D. V. Semikoz, Nonequilibrium corrections to the spectra of massless neutrinos in the early universe, *Nucl. Phys. B* **503**, 426 (1997), arXiv:hep-ph/9703315.
- [43] G. Mangano, G. Miele, S. Pastor, and M. Peloso, A Precision calculation of the effective number of cosmological neutrinos, *Phys. Lett. B* **534**, 8 (2002), arXiv:astro-ph/0111408.
- [44] G. Mangano, G. Miele, S. Pastor, T. Pinto, O. Pisanti, and P. D. Serpico, Relic neutrino decoupling including flavor oscillations, *Nucl. Phys. B* **729**, 221 (2005), arXiv:hep-ph/0506164.
- [45] P. F. de Salas and S. Pastor, Relic neutrino decoupling with flavour oscillations revisited, *JCAP* **07**, 051 (2016), arXiv:1606.06986 [hep-ph].

- [46] M. Ovchynnikov and V. Syvolap, How new physics affects primordial neutrinos decoupling: Direct simulation Monte Carlo approach, *Phys. Rev. D* **111**, 063527 (2025), arXiv:2409.07378 [astro-ph.CO].
- [47] M. Ovchynnikov and V. Syvolap, Primordial Neutrinos and New Physics: Novel Approach to Solving the Neutrino Boltzmann Equation, *Phys. Rev. Lett.* **134**, 101003 (2025), arXiv:2409.15129 [hep-ph].
- [48] O. Ihnatenko and M. Ovchynnikov, Precision calculation of N_{eff} with Neutrino Direct Simulation Monte Carlo, (2025), arXiv:2508.08379 [hep-ph].
- [49] K. Akita, G. Baur, M. Ovchynnikov, T. Schwetz, and V. Syvolap, New Physics Decaying into Metastable Particles: Impact on Cosmic Neutrinos, *Phys. Rev. Lett.* **134**, 121001 (2025), arXiv:2411.00892 [hep-ph].
- [50] K. Akita, G. Baur, M. Ovchynnikov, T. Schwetz, and V. Syvolap, Dynamics of metastable standard model particles from long-lived particle decays in the MeV primordial plasma, *Phys. Rev. D* **111**, 063542 (2025), arXiv:2411.00931 [hep-ph].
- [51] P. J. E. Peebles, Recombination of the Primeval Plasma, *Astrophys. J.* **153**, 1 (1968).
- [52] Y. B. Zeldovich and R. A. Sunyaev, The Interaction of Matter and Radiation in a Hot-Model Universe, *Astrophys. Space Sci.* **4**, 301 (1969).
- [53] B. W. Lee and S. Weinberg, Cosmological Lower Bound on Heavy-Neutrino Masses, *Phys. Rev. Lett.* **39**, 165 (1977).
- [54] P. Gondolo and G. Gelmini, Cosmic abundances of stable particles: Improved analysis, *Nucl. Phys. B* **360**, 145 (1991).
- [55] D. A. Dicus, E. W. Kolb, A. M. Gleeson, E. C. G. Sudarshan, V. L. Teplitz, and M. S. Turner, Primordial Nucleosynthesis Including Radiative, Coulomb, and Finite Temperature Corrections to Weak Rates, *Phys. Rev. D* **26**, 2694 (1982).
- [56] M. A. Herrera and S. Hacyan, Relaxation Time of Neutrinos in the Early Universe, *Astrophys. J.* **336**, 539 (1989).
- [57] M. A. Herrera and S. Hacyan, Interaction between matter and radiation at very high temperatures: I. Compton scattering, *Physics of Fluids* **28**, 3253 (1985).
- [58] N. C. Rana and B. M. Seifert, Effect of neutrino heating in the early universe on neutrino decoupling temperatures and nucleosynthesis, *Phys. Rev. D* **44**, 393 (1991).
- [59] M. Escudero, Neutrino decoupling beyond the Standard Model: CMB constraints on the Dark Matter mass with a fast and precise N_{eff} evaluation, *JCAP* **02**, 007 (2019), arXiv:1812.05605 [hep-ph].
- [60] M. Escudero Abenza, Precision early universe thermodynamics made simple: N_{eff} and neutrino decoupling in the Standard Model and beyond, *JCAP* **05**, 048 (2020), arXiv:2001.04466 [hep-ph].
- [61] A.-K. Burns, T. M. P. Tait, and M. Valli, PRyMordial: the first three minutes, within and beyond the standard model, *Eur. Phys. J. C* **84**, 86 (2024), arXiv:2307.07061 [hep-ph].
- [62] C. Giovanetti, M. Lisanti, H. Liu, S. Mishra-Sharma, and J. T. Ruderman, LINX: A Fast, Differentiable, and Extensible Big Bang Nucleosynthesis Package, *Phys. Rev. D* **112**, 063531 (2025), arXiv:2408.14538 [astro-ph.CO].
- [63] M. Escudero, G. Jackson, M. Laine, and S. Sandner, Fast and Flexible Neutrino Decoupling Part II: Beyond the Standard Model, (2026), in preparation.
- [64] O. Pisanti, A. Cirillo, S. Esposito, F. Iocco, G. Mangano, G. Miele, and P. D. Serpico, PArthENoPE: Public Algorithm Evaluating the Nucleosynthesis of Primordial Elements, *Comput. Phys. Commun.* **178**, 956 (2008), arXiv:0705.0290 [astro-ph].
- [65] R. Consiglio, P. F. de Salas, G. Mangano, G. Miele, S. Pastor, and O. Pisanti, PArthENoPE reloaded, *Comput. Phys. Commun.* **233**, 237 (2018), arXiv:1712.04378 [astro-ph.CO].
- [66] A. Arbey, AlterBBN: A program for calculating the BBN abundances of the elements in alternative cosmologies, *Comput. Phys. Commun.* **183**, 1822 (2012), arXiv:1106.1363 [astro-ph.CO].
- [67] K. Akita and M. Yamaguchi, A precision calculation of relic neutrino decoupling, *JCAP* **08**, 012 (2020), arXiv:2005.07047 [hep-ph].
- [68] J. Froustey, C. Pitrou, and M. C. Volpe, Neutrino decoupling including flavour oscillations and primordial nucleosynthesis, *JCAP* **12**, 015 (2020), arXiv:2008.01074 [hep-ph].
- [69] J. J. Bennett, G. Buldgen, P. F. De Salas, M. Drewes, S. Gariazzo, S. Pastor, and Y. Y. Y. Wong, Towards a precision calculation of N_{eff} in the Standard Model II: Neutrino decoupling in the presence of flavour oscillations and finite-temperature QED, *JCAP* **04**, 073 (2021), arXiv:2012.02726 [hep-ph].
- [70] S. Gariazzo, P. F. de Salas, and S. Pastor, Thermalisation of sterile neutrinos in the early Universe in the 3+1 scheme with full mixing matrix, *JCAP* **07**, 014 (2019), arXiv:1905.11290 [astro-ph.CO].
- [71] A. F. Heckler, Astrophysical applications of quantum corrections to the equation of state of a plasma, *Phys. Rev. D* **49**, 611 (1994).
- [72] N. Fornengo, C. W. Kim, and J. Song, Finite temperature effects on the neutrino decoupling in the early universe, *Phys. Rev. D* **56**, 5123 (1997), arXiv:hep-ph/9702324.
- [73] J. J. Bennett, G. Buldgen, M. Drewes, and Y. Y. Y. Wong, Towards a precision calculation of the effective number of neutrinos N_{eff} in the Standard Model I: the QED equation of state, *JCAP* **03**, 003 (2020), [Addendum: JCAP 03, A01 (2021)], arXiv:1911.04504 [hep-ph].
- [74] J. I. Kapusta, Quantum chromodynamics at high temperature, *Nucl. Phys. B* **148**, 461 (1979).
- [75] G. Jackson and M. Laine, QED corrections to the thermal neutrino interaction rate, *JHEP* **05**, 089 (2024), arXiv:2312.07015 [hep-ph].

- [76] G. Jackson and M. Laine, $\nu\bar{\nu}$ production, annihilation, and scattering at MeV temperatures and NLO accuracy, *JCAP* **05**, 054 (2025), arXiv:2412.03958 [hep-ph].
- [77] G. Sigl and G. Raffelt, General kinetic description of relativistic mixed neutrinos, *Nucl. Phys. B* **406**, 423 (1993).
- [78] S. Navas *et al.* (Particle Data Group), Review of particle physics, *Phys. Rev. D* **110**, 030001 (2024).
- [79] D. Nötzold and G. Raffelt, Neutrino dispersion at finite temperature and density, *Nucl. Phys. B* **307**, 924 (1988).
- [80] I. Esteban, M. C. Gonzalez-Garcia, M. Maltoni, I. Martinez-Soler, J. P. Pinheiro, and T. Schwetz, NuFit-6.0: updated global analysis of three-flavor neutrino oscillations, *JHEP* **12**, 216 (2024), arXiv:2410.05380 [hep-ph].
- [81] V. Domcke, M. Escudero, M. Fernandez Navarro, and S. Sandner, Lepton flavor asymmetries: from the early Universe to BBN, *JHEP* **06**, 137 (2025), arXiv:2502.14960 [hep-ph].
- [82] V. Domcke, M. Escudero, M. Fernandez Navarro, and S. Sandner, A Limit on the Total Lepton Number in the Universe from BBN and the CMB, (2025), arXiv:2510.02438 [hep-ph].
- [83] J. R. Bond, G. M. Fuller, E. Grohs, J. Meyers, and M. J. Wilson, Cosmic neutrino decoupling and its observable imprints: insights from entropic-dual transport, *JCAP* **09**, 014 (2024), arXiv:2403.19038 [astro-ph.CO].
- [84] J. Erler and S. Su, The Weak Neutral Current, *Prog. Part. Nucl. Phys.* **71**, 119 (2013), arXiv:1303.5522 [hep-ph].
- [85] J. Bernstein, *Kinetic theory in the expanding universe*, Cambridge Monographs on Mathematical Physics (Cambridge University Press, Cambridge, U.K., 1988).
- [86] D. J. Fixsen, The Temperature of the Cosmic Microwave Background, *Astrophys. J.* **707**, 916 (2009), arXiv:0911.1955 [astro-ph.CO].
- [87] R. R. Parwani and C. Corianò, Higher-order corrections to the equation-of-state of QED at high temperature, *Nucl. Phys. B* **434**, 56 (1995), arXiv:hep-ph/9409269.
- [88] P. B. Arnold and C. Zhai, Three-loop free energy for high-temperature QED and QCD with fermions, *Phys. Rev. D* **51**, 1906 (1995), arXiv:hep-ph/9410360.
- [89] C. Zhai and B. M. Kastening, Free energy of hot gauge theories with fermions through g^5 , *Phys. Rev. D* **52**, 7232 (1995), arXiv:hep-ph/9507380.
- [90] S. Chandrasekhar, *An introduction to the study of stellar structure* (University of Chicago Press, Chicago, U.S., 1939).